

Review

Recent Progress in g-C₃N₄-Based Photocatalysts for Organic Pollutant Degradation: Strategies to Improve Photocatalytic Activity

Yang Ruan ¹, Yuanan Hu ¹ and Hefa Cheng ^{2,*}

¹ MOE Laboratory of Groundwater Circulation and Evolution, School of Water Resources and Environment, China University of Geosciences (Beijing), Beijing 100083, China; ryan-yruan@outlook.com (Y.R.); yhu@cugb.edu.cn (Y.H.)

² MOE Key Laboratory for Earth Surface Processes, College of Urban and Environmental Sciences, Peking University, Beijing 100871, China

* Correspondence: hefac@umich.edu; Tel.: +86-10-6276-1070

Abstract: With unique photochemical properties, graphitic carbon nitride (g-C₃N₄) has gained significant attention for application in photocatalytic degradation of a wide range of organic pollutants. However, its performance is limited by the rapid electron–hole recombination and the relatively weak redox capability. Substantial progress has been made in the preparation of g-C₃N₄-based photocatalysts with enhanced photocatalytic activity. This review summarizes the recent advances in strategies to improve the photocatalytic activity of g-C₃N₄-based photocatalysts and their application in the photocatalytic degradation of organic pollutants. Morphology control, doping, functionalization, metal deposition, dye sensitization, defect engineering, and construction of heterojunctions can be used to improve the photocatalytic activity of g-C₃N₄ through promoting charge carrier separation, reducing the bandgap, and suppressing charge recombination. Furthermore, a range of oxidants, such as hydrogen peroxide and persulfate, can be coupled with g-C₃N₄-based photocatalysts to enhance the generation of reactive oxygen species and boost the photocatalytic degradation of organic pollutants. Precise control over the g-C₃N₄ structure during the synthesis process remains a challenge, and further improvements are required in photocatalyst stability and the mineralization rates of organic pollutants. More research and development effort is needed to address the existing challenges, refine the design of g-C₃N₄-based photocatalysts to improve their activity, and promote their practical application in pollutant degradation.

Keywords: graphitic carbon nitride; photocatalytic degradation; structural modification; heterojunction; photo-generated carrier separation



Academic Editors: Detlef W. Bahnemann, Jorge Bedia, Magdalena Janus and Christos Trapalis

Received: 31 December 2024

Revised: 28 January 2025

Accepted: 2 February 2025

Published: 4 February 2025

Citation: Ruan, Y.; Hu, Y.; Cheng, H. Recent Progress in g-C₃N₄-Based Photocatalysts for Organic Pollutant Degradation: Strategies to Improve Photocatalytic Activity. *Catalysts* **2025**, *15*, 148. <https://doi.org/10.3390/catal15020148>

Copyright: © 2025 by the authors. Licensee MDPI, Basel, Switzerland. This article is an open access article distributed under the terms and conditions of the Creative Commons Attribution (CC BY) license (<https://creativecommons.org/licenses/by/4.0/>).

1. Introduction

With the sustained global economic growth in recent years, wastewater pollution due to rapid industrialization and urbanization has caused great concern. A wide variety of organic chemicals, including antibiotics, dyes, pharmaceutical and personal care products, pesticides, and flame retardants, contribute to the pollution of wastewater through their production and use in factories [1,2]. These organic pollutants in wastewaters are typically not effectively degraded in the conventional wastewater treatment processes [3]. The development of green and efficient methods for their removal has become a growing area of research. Advanced oxidation processes (AOPs) with superior oxidation capability are considered a promising technology for addressing the issue of organic pollutants in

wastewater [4]. The remarkable reactivity of AOPs arises from the generation of reactive oxygen species (ROs), such as superoxide radicals ($\bullet\text{O}_2^-$), hydroxyl radicals ($\bullet\text{OH}$), sulfate radicals ($\text{SO}_4\bullet^-$), and singlet oxygen ($^1\text{O}_2$). Under the attack of these strong oxidants, most organic pollutants can be broken down into degradation intermediates, and even partially or fully mineralized into H_2O and CO_2 [5,6].

A variety of AOPs have been put forward to use for the degradation of organic wastewater [7,8]. Benefiting from the plentiful and renewable solar energy on Earth, as well as its cost-effectiveness, environmental friendliness, high efficiency, and mild reaction conditions, photocatalytic oxidation is widely regarded as a highly promising and sustainable solution for degrading organic pollutants [9,10]. As shown in Figure 1a, photocatalytic reactions consist of three key steps. Initially, the photocatalyst absorbs photons with energy ($h\nu$) greater than or equal to its bandgap energy (E_g), leading to the generation of electron–hole pairs. Subsequently, the photo-generated charge carriers separate and then migrate to the surface of the photocatalyst. Electrons that move from the valence band (VB) to the conduction band (CB) are referred to as photo-generated electrons (e^-), while the remaining holes in the VB are known as photo-generated holes (h^+). Finally, they react directly or indirectly with the organic pollutants on the surface of the photocatalysts [11,12]. The stability and efficiency of photocatalytic reactions depend on the effective design and precise fabrication of photocatalysts.

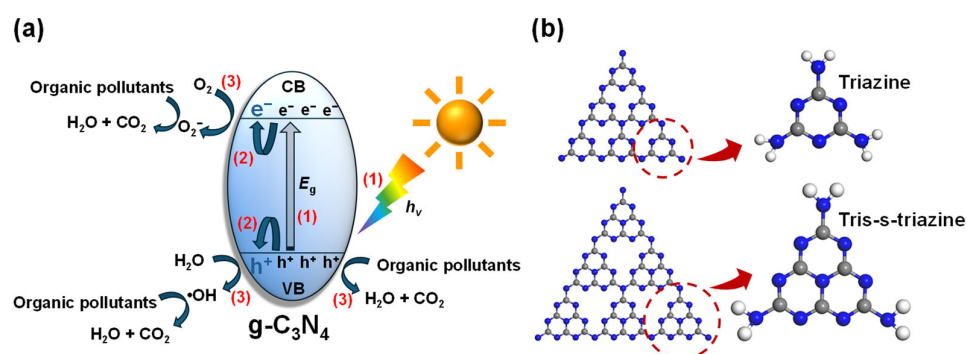


Figure 1. Schematic illustration of the photocatalytic reaction (a) and the basic structural unit (b) of $g\text{-C}_3\text{N}_4$. The numbers in red denote the three key steps in photocatalytic reactions.

Among various types of photocatalysts, graphitic carbon nitride ($g\text{-C}_3\text{N}_4$), a non-metallic semiconductor, has received significant interest globally. As shown in Figure 1b, triazine (C_3N_3) rings and tri-*s*-triazine (C_6N_7) rings are the basic structural units of $g\text{-C}_3\text{N}_4$. The latter is the most stable phase, making it the typical structural unit that forms $g\text{-C}_3\text{N}_4$. Due to its suitable bandgap (ca. 2.7 eV) and favorable band position, $g\text{-C}_3\text{N}_4$ exhibits high visible light responsiveness. It also offers a range of benefits, such as low cost, excellent stability, and environmental friendliness, making it a promising non-metallic semiconductor photocatalyst [13,14].

Despite its advantages, the pristine $g\text{-C}_3\text{N}_4$ photocatalyst has several limitations, including a relatively small specific surface area (SSA), easy recombination of photo-generated charge carriers, and weak redox capability. These drawbacks greatly limit its large-scale application [15]. To date, various strategies have been employed to boost the photocatalytic performance of $g\text{-C}_3\text{N}_4$ [16,17].

Some excellent reviews on the synthesis and design strategies of $g\text{-C}_3\text{N}_4$ -based photocatalysts have been published [15,18,19]. However, strategies to enhance the efficiency of $g\text{-C}_3\text{N}_4$ -based photocatalysts for the degradation of organic pollutants have not been systematically reviewed, and the advantages and disadvantages of different design strategies for $g\text{-C}_3\text{N}_4$ -based photocatalysts have not been compared. In this review, recent advances

in design strategies aimed at boosting the photocatalytic activity of g-C₃N₄-based photocatalysts are comprehensively discussed, while the strategy of oxidant coupling to further enhance photocatalytic degradation of organic pollutants is also introduced. Finally, the perspectives and challenges of g-C₃N₄-based photocatalysts in degrading organic pollutants are discussed. By systematically summarizing the major strategies for improving the photocatalytic activity of g-C₃N₄-based photocatalysts, along with their respective advantages and limitations, we hope that this review can provide valuable guidance and insights for the development of more efficient photocatalysts. We also aim to inspire future work to address the existing challenges, refine the design of g-C₃N₄-based photocatalysts, and promote their practical application in pollution control.

2. Strategies to Improve Photocatalytic Activity

Numerous strategies have been proposed to enhance the photocatalytic activity of g-C₃N₄-based photocatalysts through suppressing the recombination of photo-generated carriers, optimizing charge migration pathway, promoting the separation of photo-generated carriers, and adjusting their redox capability. This section systematically introduces these strategies, including morphology control, doping, functionalization, metal deposition, dye sensitization, defect engineering, and construction of heterojunctions. Table 1 compares the major advantages and limitation of these strategies for enhancing the photocatalytic activity of g-C₃N₄-based photocatalysts. Interestingly, these strategies may work synergistically in practical application. For instance, the formation of heterojunctions may involve the combination of semiconductors with different dimensional morphology, and the incorporation of foreign elements is often associated with the formation of surface defects.

Table 1. Summary of major advantages and limitations of different strategies to improve photocatalytic activity of g-C₃N₄-based photocatalysts.

Strategy	Advantages	Limitations
Morphology control	Various morphology can be chosen to meet different application requirements, and the modification process is highly adaptable.	Precise control over the morphology and size remains a challenge.
Doping	The doping procedure is simple and easy to implement.	Certain dopants may result in a decrease in specific surface area, and may increase potential risk from metal leaching.
Functionalization	The required properties can be selectively introduced through various functional groups.	Most functionalization methods are not environmentally friendly, and g-C ₃ N ₄ functionalized with non-covalent groups tends to exhibit poor stability.
Metal deposition	The localized surface plasmon resonance effect can expand the light absorption range, and the formation of a Schottky barrier can accelerate electron transfer.	Noble metals are expensive.
Dye sensitization	The dye can be designed and synthesized in a controlled manner, with adjustments to the appropriate CB and light absorption range.	The sensitizing dye may decompose during photocatalytic degradation process.
Defect engineering	Vacancies adjust the energy band alignment and create trap states that enhance charge carrier separation and transfer.	Excess defects narrow the bandgap, reduce the redox capacity of charge carriers, and increase their recombination.
Construction of heterojunctions	Significantly enhances electron–hole pair separation and reduces their recombination.	Precise control of material interfaces is required in constructing heterojunction photocatalysts.

2.1. Morphology Control

$g\text{-C}_3\text{N}_4$ with various morphology has been constructed. According to their dimensions, $g\text{-C}_3\text{N}_4$ -based photocatalysts have been fabricated as zero-dimensional (0D) nanostructures (e.g., quantum dots [20]), one-dimensional (1D) nanostructures (e.g., nanorods [21], nanowires [22], nanobelts [23], and nanotubes [24]), two-dimensional (2D) nanostructures (e.g., nanosheets [25]), and three-dimensional (3D) nanostructures (e.g., nanoflowers [26], nanospheres [27], nanocages [28], and hierarchical structures [29]).

Controlled morphology imparts various advantages and properties to $g\text{-C}_3\text{N}_4$. The 0D structure of $g\text{-C}_3\text{N}_4$ generally refers to $g\text{-C}_3\text{N}_4$ quantum dots (QDs). This unique structure endows the photocatalyst with excellent light absorption capability, superior conversion efficiency, and enhanced photocatalytic performance [30,31]. Rajeshwari et al. [20] fabricated a $g\text{-C}_3\text{N}_4$ QD-incorporated MoO_3 catalyst, which brought about 98% degradation of *p*-chlorophenol and 89% degradation of rifampicin after 330 min of visible light irradiation. The improvement in photocatalytic activity through $g\text{-C}_3\text{N}_4$ QD doping was confirmed, which led to a notable narrowing of the band gap, better utilization of visible light, a larger surface area, an improved charge transfer rate, and reduced electron–hole pair recombination.

The formation of 1D tubular structures can provide an effective 1D pathway for photo-generated charge carriers, thereby promoting the charge transfer rate [32]. Zhang et al. [33] prepared a metal-free nanotubular carbon nitride photocatalyst (CN NT) for activating O_2 to decompose chloroquine phosphate. Density functional theory (DFT) calculations indicated that the geometric modification of CN NT optimized the surface electronic effect, particularly through enhancing charge separation and transfer properties, which promoted strong electron interactions with O_2 , thereby improving the O_2 adsorption capacity. Furthermore, CN NT exhibited enhanced charge donation and interaction with adsorbed O_2 , enabling better photocatalytic O_2 activation and the generation of ROSs.

The 2D nanosheet structure of $g\text{-C}_3\text{N}_4$ usually results in a larger SSA, providing more active sites for reactant capture and activation, and simultaneously improving mass transfer [34,35]. Additionally, the reduced thickness significantly facilitates the separation of electron–hole pairs, shortens the migration path to the surface of $g\text{-C}_3\text{N}_4$, suppresses their recombination, and improves their overall utilization [36]. Kuate et al. [37] developed a black graphite carbon nitride photocatalyst using a one-step calcination method with urea and phloxine B, and used it for degrading tetracycline (TC) in seawater under visible light. Up to 92% of TC degraded at room temperature after 2 h, which is more than that achieved by pure $g\text{-C}_3\text{N}_4$ under the same conditions. The enhanced photocatalytic performance was attributed to the ultrathin nanosheet structure, which not only minimizes the charge transfer distance but also facilitates more efficient electron–hole separation, thereby improving the overall photocatalytic degradation efficiency.

The 3D structure, with its simple synthesis process, outstanding absorption of visible light, and recyclability, endows $g\text{-C}_3\text{N}_4$ with significant potential for engineering application [30,38]. Gnanaguru et al. [39] fabricated a 3D $g\text{-C}_3\text{N}_4/\text{WS}_2/\text{agarose}$ aerogel (GCWAA) using a simple freeze-casting method. The synthesized 3D GCWAA exhibited promising photocatalytic removal of tetracycline, ofloxacin, and sulfamethoxazole, with degradation rates reached 94%, 96%, and 97%, respectively, in 90 min. The lightweight nature and tunable hydrophobicity of the 3D aerogel structure allow it to float on water surfaces, enhancing its ability to absorb the incident light and facilitating recovery and reuse.

In summary, the morphology of $g\text{-C}_3\text{N}_4$ influences its key physical and photochemical properties, such as SSA, light absorption capacity, charge carrier dynamics, and ultimately, photocatalytic performance. For instance, specific morphology increases the SSA of $g\text{-C}_3\text{N}_4$ -based photocatalysts and provides more active sites for reactions to enhance the

photocatalytic degradation performance. Moreover, the morphology affects the separation and transportation of photo-generated electron–hole pairs. For example, tubular structures provide an effective 1D pathway for photo-generated charge carriers and increase the charge transfer rate, reduce their recombination, and enhance photocatalytic efficiency [32]. Additionally, certain morphology, such as 3D tubular yolk–shell structures, can effectively enhance light harvesting by utilizing multiple scatterings and reflections within the yolk–shell chambers, which increases the photocatalytic activity [40]. To address the diverse needs of practical application, it is necessary to combine g-C₃N₄ with one or more strategies to achieve synergistic interactions. Structural design and morphology control of g-C₃N₄ are often adopted together to optimize the integration between components in the photocatalysts.

2.2. Doping

Modifying the bandgap structure and surface of g-C₃N₄ can drastically improve the photocatalytic efficiency of g-C₃N₄-based photocatalysts [15]. Elemental doping is considered an effective strategy to modify the bandgap and electronic structure of g-C₃N₄, as it can efficiently narrow the bandgap, improve light absorption, and adjust the redox potential of g-C₃N₄ [41,42]. As shown in Figure 2a, doping involves introducing foreign elements into the semiconductor, where the introduced elements can occupy structural voids within g-C₃N₄ or substitute its carbon or nitrogen atoms [34]. Bandgap engineering through metal doping [43], non-metal doping [44], or their co-doping [45] has proven to be an effective strategy for tailoring g-C₃N₄ for photocatalytic application [34]. Table 2 summarizes the enhancement in photocatalytic performance of g-C₃N₄-based photocatalysts through the introduction of common doped elements.

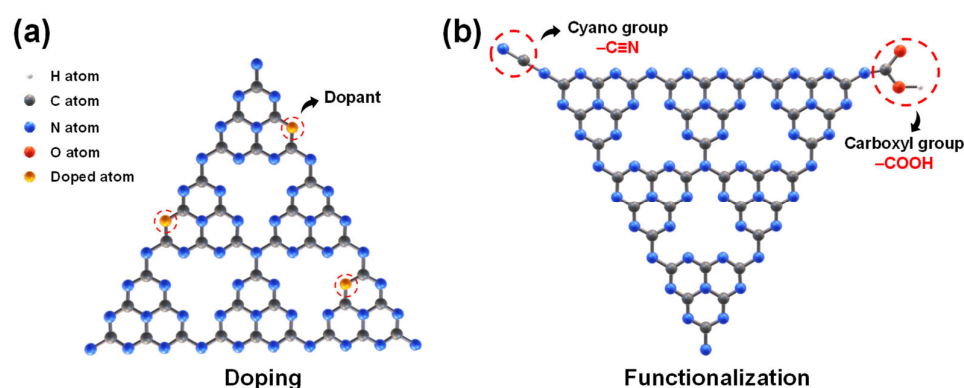


Figure 2. Schematic diagram of doping (a) and functionalization of g-C₃N₄ (b).

Table 2. Summary of enhancement in photocatalytic activity of g-C₃N₄-based photocatalysts by different doped elements.

Doped Element	Pollutant	Concentration (mg L ⁻¹)	Degradation Efficiency	Kinetic Constant <i>k</i> (min ⁻¹)	Enhancement Factor of <i>k</i> over Reference Photocatalyst	Reference
Li	RhB	10	98.0%	0.082	6.8 times	[46]
Na	MB	20	98.5%	0.066	3.6 times	[47]
K	TMP	100	90.8%	0.038	2.4 times	[43]
Ca	ENR	5	-	0.046	3.3 times	[48]
Mg	OTC	20	80%	0.012	2.6 times	[49]
Fe	RhB	10	100%	0.117	10 times	[50]

Table 2. Cont.

Doped Element	Pollutant	Concentration (mg L ⁻¹)	Degradation Efficiency	Kinetic Constant <i>k</i> (min ⁻¹)	Enhancement Factor of <i>k</i> over Reference Photocatalyst	Reference
Co	MB	10	96%	0.013	1.7 times	[51]
Ni	TC	10	77%	0.006	2.8 times	[52]
Cu	IBP	5	93%	0.089	2.3 times	[53]
Ag	RhB	10	97.2%	0.205	4.9 times	[54]
B	4-CP	20	100%	0.092	4.9 times	[55]
C	BPA	10	96%	0.053	10.6 times	[56]
O	2,4-DNP	10	100%	0.038	1.6 times	[57]
N	TC	20	93%	0.135	8.5 times	[58]
S	ATZ	2	99.6%	0.046	2.4 times	[59]
P	2,4-D	1	90%	0.043	4.0 times	[60]
F	TC	10	99.8%	0.021	1.7 times	[61]
Cl	TC	10	92%	0.020	5.2 times	[62]
Br	OTC	10	75%	0.018	4.3 times	[63]
I	TC	10	99.8%	0.032	2.6 times	[64]

Note: RhB = rhodamine B; MB = methyl blue; TMP = trimethoprim; ENR = enrofloxacin; OTC = oxytetracycline; TC = tetracycline; IBP = Ibuprofen; 4-CP = 4-chlorophenol; BPA = bisphenol A; 2,4-DNP = 2,4-dinitrophenol; ATZ = atrazine; 2,4-D = 2,4-dichlorophenoxyacetic acid; “-” indicates missing data in the reference.

The metal dopants that are currently applied to g-C₃N₄-based photocatalysts are primarily alkali metals and transition metals, which can be further categorized into s-block metals (Li [46], Na [47], K [43], Ca [48], Mg [65]), d-block metals (Fe [66], Co [67], Ni [68]), and ds-block metals (Cu [69], Ag [54]). The incorporation of metal elements plays a key role in boosting charge carrier separation and enhancing visible light absorption, ultimately improving the photocatalytic efficiency [70]. Mao et al. [66] successfully assembled an iron-doped g-C₃N₄/GO hybrid composite (GO/Fe-GCN) and employed it as an adsorption-photocatalytic Fenton-type heterogeneous catalyst. The experimental results showed that Fe²⁺ and Fe³⁺ were captured by the nitrogen-rich g-C₃N₄, resulting in the formation of well-dispersed active sites. The equilibrium removal rate of Rhodamine B reached 83.6%, which is five times higher than that of the pristine g-C₃N₄. The hybrid GO/Fe-GCN structure, along with the efficient cycling of Fe²⁺/Fe³⁺, plays a crucial role in the synergistic effect of adsorption enrichment and the photocatalytic Fenton reaction. Furthermore, the Fe–N ligands that are formed through Fe doping facilitate charge carrier migration while reduce their recombination.

Numerous non-metal elements have been extensively employed for doping g-C₃N₄-based photocatalysts, including B [55], C [56], O [71], N [58], S [59], P [60], F [61], Cl [62], Br [63], and I [64]. These elements can adjust the electronic structure of g-C₃N₄-based photocatalysts, leading to enhanced photocatalytic activity. Meng et al. [71] synthesized O-doped porous g-C₃N₄ (OCN) through a thermal polymerization method for the activation of peroxymonosulfate (PMS) to remove carbamazepine (CBZ) under visible light and dark conditions. Their findings revealed that the oxygen atoms facilitated electron transfer by tuning the electronic structure of g-C₃N₄, activating PMS even without light irradiation. Moreover, the incorporation of oxygen atoms narrowed the bandgap, improving the light responsiveness and enhancing the efficiency of electron–hole pair separation, which in turn boosted the photocatalytic activation efficiency of OCN.

Co-doping involves the incorporation of two or more metal or non-metal elements into a material, resulting in enhanced photocatalytic performance through synergistic interactions. Compared to single-element doping, co-doping typically achieves superior photocatalytic activity [45,72–74]. Yue et al. [72] synthesized potassium and sodium co-doped carbon nitride (CN-K/Na) through ionothermal polymerization of urea. This co-doping process altered the crystallinity and surface morphology of the carbon nitride. The simultaneous introduction of K and Na significantly promoted the formation of long-range ordered crystalline structure in carbon nitride, outperforming single-element doping. In addition, the CN-K/Na co-doped carbon nitride possessed substantial amount of surface $-\text{C}\equiv\text{N}$ and $-\text{NH}_2$ functional groups, which play a crucial role in enhancing photocatalytic performance. This improvement in activity is driven by multiple mechanisms: the Na^+ ions aid in the transfer of charges within the plane of the material, while K^+ ions support charge migration between different planes. In addition, the $-\text{C}\equiv\text{N}$ groups are instrumental in capturing and activating O_2 , while the $-\text{NH}_2$ groups facilitate the extraction and release of protons.

2.3. Functionalization

The use of various chemical modifiers for functionalization has proven to be an effective approach to introducing new features into $\text{g-C}_3\text{N}_4$. Through molecular doping, functionalization can optimize the energy band structure, photoelectrochemical properties, and intrinsic conjugation system of $\text{g-C}_3\text{N}_4$. Owing to its conjugated structure, the physicochemical properties of $\text{g-C}_3\text{N}_4$ can be significantly altered by copolymerizing with unique aromatic groups or organic units [75–77]. The functionalization of $\text{g-C}_3\text{N}_4$ typically refers to covalent modification, where new functional groups are introduced through stable covalent bonds between the $\text{g-C}_3\text{N}_4$ structure and chemical modifiers. Figure 2b shows a schematic diagram for the functionalization of $\text{g-C}_3\text{N}_4$ using the cyano and carboxyl groups, with the introduction of these groups imparting new properties to $\text{g-C}_3\text{N}_4$.

A common covalent functionalization strategy is oxidation, which incorporates one or more oxygen-containing functional groups, such as hydroxyl groups, carboxyl groups, and others, onto the surface of $\text{g-C}_3\text{N}_4$. This process can adjust its band structure, thereby influencing the types of reactive species that are generated during photocatalysis and controlling the degradation and transformation pathways of pollutants [78,79]. Ming et al. [80] employed a simple hydrothermal method to gradually oxidize $\text{g-C}_3\text{N}_4$, resulting in oxidized $\text{g-C}_3\text{N}_4$ (CNO). Besides the N–O groups, the formation of C=O and C–O groups was also detected in the CNO, and the introduction of these electron-withdrawing groups reduced the VB level of $\text{g-C}_3\text{N}_4$, thereby enhancing its photo-oxidation activity. Furthermore, the photocurrent response of CNO was measured to be approximately 10 times higher than that of raw $\text{g-C}_3\text{N}_4$, and the photocatalytic activity of CNO for the degradation of Acid Orange 7 was found to be approximately 7 times higher than that of $\text{g-C}_3\text{N}_4$. Together, the incorporation of these oxygen-containing functional groups plays a significant role in improving the separation efficiency of photo-generated electrons and holes, thus enhancing the photocatalytic activity of CNO.

In addition, a variety of functional groups, such as cyano groups [81], amino groups [82], aldehyde groups [83], and amidoxime groups [84], have been used for the functionalization of $\text{g-C}_3\text{N}_4$ to regulate its photocatalytic activity. Xu et al. [81] found that the introduction of the cyano group increased the local charge density of $\text{g-C}_3\text{N}_4$, creating a potential well that attracted exciton “holes”, thereby accelerating exciton dissociation. As a result, free radical selectivity up to 97.6% was achieved in the photocatalytic degradation of tetracycline, with the removal of total organic carbon reached 82.1% within 6 h. This approach, which selectively generates radicals with stronger photocatalytic oxidation abil-

ity by manipulating charge carrier transfer and exciton dissociation processes, provides a method for the precise control of radical production to mineralize refractory pollutants.

g-C₃N₄ has also been functionalized using non-covalent methods. Unlike covalent bonding, non-covalent methods primarily rely on physical bonding and intermolecular interactions, including electrostatic interactions, van der Waals interactions, and π - π interactions [85]. Chen et al. [86] utilized an ultrasonic dispersion method to hybridize Cu(II) meso-Tetra (4-carboxyphenyl) porphyrin (CuTCPP) with g-C₃N₄ through π - π interactions. The resulting composite possessed significantly enhanced photocatalytic activity under visible light compared to pristine g-C₃N₄. This improvement was attributed to the efficient transfer of electrons from CuTCPP to g-C₃N₄, which facilitated the separation and migration of photo-generated electron-hole pairs. Notably, the photocatalytic activity of the composite reached its maximum at the CuTCPP content of 0.75%, with the rate constant for phenol degradation being approximately 2.2 times that of g-C₃N₄. The enhanced photocatalytic performance under visible light irradiation is ascribed not only to the well-matched overlapping band structures, which promote the separation and transfer of electron-hole pairs, but also to the sensitization effect of CuTCPP, which leads to an overall improvement in the photocatalytic activity of g-C₃N₄ across its full absorption spectrum.

It is noteworthy that non-covalent interactions are weaker than covalent bonds, resulting in composites with relatively poor stability. However, non-covalent methods can retain the inherent properties of both components while incorporating their characteristics [87]. Therefore, in practical application, the choice of an appropriate functionalization method should be based on the specific requirements.

2.4. Metal Deposition

Metal doping incorporates metals into the structure of g-C₃N₄, whereas metal deposition places metals onto the surface of g-C₃N₄. Figure 3 schematically illustrates metal deposition on g-C₃N₄. When the metal interfaces with the g-C₃N₄ surface, owing to the higher Fermi energy (E_f) of the g-C₃N₄ compared to the metal, photo-generated electrons will migrate from the higher E_f of g-C₃N₄ to the metal, forming a Schottky barrier [88]. As a result, the structure comprising of g-C₃N₄ and the metal is referred to as a Schottky junction. Depositing metal onto the surface of g-C₃N₄ can promote the separation of photo-generated charge carriers and enhance the photocatalytic activity [89,90]. Additionally, the localized surface plasmon resonance (LSPR) effect leads to the plasmonic electron injecting to g-C₃N₄, extending photocatalyst's light absorption range [91,92]. Since they can promote photocatalytic reactions, the doped metals are also referred to as cocatalysts. Based on the aforementioned principles, the deposition of noble metals, such as Au [93], Ag [94], Pt [95], and Pd [96], has been widely studied and proven to be an efficient method for enhancing the solar energy utilization capability of g-C₃N₄. Nevertheless, the high cost and limited availability of noble metals restrict their practical utilization. Consequently, many researchers have explored the deposition of non-noble metals, such as Ni [97], Cu [98], and Bi [99], to strengthen the photocatalytic performance of g-C₃N₄-based catalysts. The LSPR effect of non-noble metals can also elevate the separation and migration efficiency of electron-hole pairs and expand the absorption range of photocatalysts. However, their free carrier density is significantly lower compared to the noble metals, and their LSPR frequency corresponds to longer wavelength, resulting in lower photocatalytic activity, which limits their further development [100].

2.5. Dye Sensitization

Dyes possess high tendency for light absorption and can efficiently convert longer wavelength solar light into molecular energy [101]. Therefore, dye sensitization is an

effective method for enabling g-C₃N₄-based photocatalysts to capture solar energy from longer wavelength. As shown in Figure 4, when the CB of g-C₃N₄ lies between the LUMO and HOMO levels of the dye, the electrons that are generated upon light excitation of the dye on g-C₃N₄ can transfer from the LUMO orbitals of the dye to the CB of the g-C₃N₄. This not only broadens the light absorption range, but also suppresses the carrier recombination, thus enhancing the photocatalytic activity [102]. Since dyes are organic molecules that can be designed and synthesized in a controllable manner [102], it is easy to obtain dyes with suitable CB values and tunable absorption range. Two common types of dyes that have been used for sensitization of g-C₃N₄ are metal-free dyes and metal-based dyes. Bakhtiar et al. [103] utilized a hydrothermal technique to load zinc phthalocyanine (ZnPc) onto the surface of g-C₃N₄, significantly boosting its photocatalytic capability. Within 1 h of light irradiation, 85% of 2,4-dichlorophenol degraded in the presence of the ZnPc-functionalized g-C₃N₄. Its high photocatalytic activity was attributed to the excellent visible light absorption and efficient generation of superoxide ions and holes, which were generated through charge transfer between g-C₃N₄ and ZnPc. However, during the photocatalytic degradation process, the free radicals generated may indiscriminately oxidize the sensitizing dye. As a result, dye sensitization is more commonly applied in photocatalytic hydrogen production rather than in the photocatalytic degradation of organic pollutants.

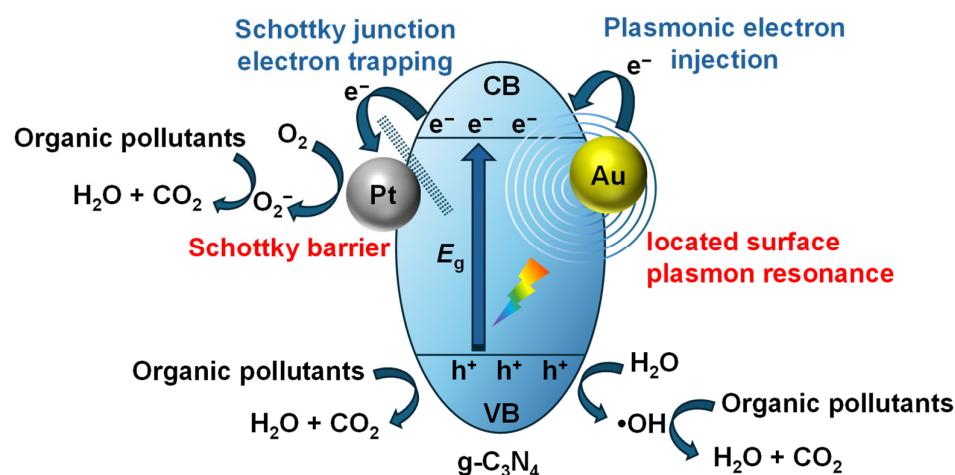


Figure 3. Schematic illustration of metal deposition (using Pt and Au as examples) for boosting the photocatalytic activity of g-C₃N₄.

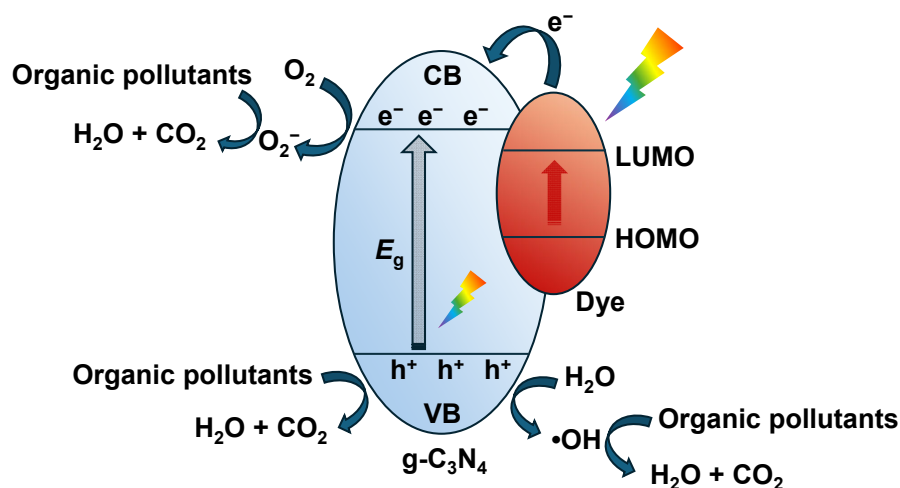


Figure 4. Mechanisms for sensitizing g-C₃N₄-based photocatalysts using dyes. The red arrow indicates the transition of electrons from HOMO to LUMO after light excitation of the dye.

2.6. Defect Engineering

When the periodic arrangement of atoms or ions in a crystalline structure alters, defects are introduced into the material, which are referred to as crystallographic defects [104]. Since defects can be precisely introduced and characterized, defect engineering can be utilized to optimize the performance of $g\text{-C}_3\text{N}_4$ -based photocatalysts by improving charge transfer and separation, enhancing light absorption, or manipulating surface reactions [105]. Generally, defects in $g\text{-C}_3\text{N}_4$ are point defects, which can be categorized into four distinct types: nitrogen vacancies [106], carbon vacancies [107], amino defects [108], and cyano defects [109,110]. Introducing vacancies into semiconductors can narrow their band gap, thereby expanding the photocatalyst's light absorption range [111]. Li et al. [112] constructed porous $g\text{-C}_3\text{N}_4$ nanosheets with carbon vacancies through a simple annealing process. In the photocatalytic Fenton-like reaction, the degradation efficiency of metronidazole reached 90.7%, and the TOC removal efficiency achieved 62% within 100 min, which was approximately 6 times higher than those achieved by $g\text{-C}_3\text{N}_4$. The results indicated that carbon vacancies could broaden the light absorption range, leading to a negative shift in the energy bands, which in turn promotes the capture of photo-generated electrons and activates the surface-adsorbed molecular oxygen. Defect-induced electronic states, commonly referred to as "trap states", play a crucial role in expanding light absorption by enabling electron excitation. Additionally, these states provide pathways for the energy relaxation of photo-generated charge carriers within VB and CB. By influencing the dynamics of charge carriers, these states accelerate the efficient separation and transport of electron-hole pairs, ultimately enhancing the photocatalytic activity. Liu et al. [113] synthesized nitrogen-defective $g\text{-C}_3\text{N}_4$ with varying nitrogen defect density for photocatalytic degradation of ciprofloxacin (CIP). The degradation rate constant of CIP in the presence of nitrogen-defective $g\text{-C}_3\text{N}_4$ was approximately an order of magnitude higher than that of $g\text{-C}_3\text{N}_4$. The incorporation of nitrogen defects induced defect states between the CB and VB, thereby modulating the electronic and band structure. These induced defect states shifted downward toward the VB, achieving an optimal nitrogen defect density to facilitate the excitation of electrons. This effectively narrowed the bandgap, broadened the light absorption range, and enhanced the separation and transfer of charge carriers.

2.7. Construction of Heterojunctions

In an isolated $g\text{-C}_3\text{N}_4$ photocatalytic system, photo-generated electrons in the CB are likely to recombine with the holes in the VB, causing electron-hole recombination, which is detrimental to the photocatalytic activity. Hence, the development of $g\text{-C}_3\text{N}_4$ -based heterostructures has garnered significant attention for promoting the photocatalytic activity of $g\text{-C}_3\text{N}_4$. These heterostructures can significantly expand the light absorption capacity, increase the SSA, and enhance the density of active sites. Additionally, the incorporation of cocatalysts helps lower the overpotential that is required for catalytic reactions and enhances the separation of photo-generated charge carriers under light excitation. In general, designing and fabricating suitable heterostructures is widely regarded as one of the most effective approaches to improve the efficiency of electron-hole pair separation, yielding a notable increase in photocatalytic activity [12]. Moreover, the introduction of other components, presumably with synergistic interactions, brings several new advantages, including enhanced light absorption capacity, higher surface reactivity, and optimized band positions, all of which benefit the photocatalytic activity. Based on the separation and transfer mechanisms of photo-generated electron-hole pairs, $g\text{-C}_3\text{N}_4$ -based heterostructures are grouped into four major types: Type-II heterojunction, Z-scheme heterojunction, S-scheme heterojunction, and p-n heterojunction.

2.7.1. Type-II Heterojunction

A conventional Type-II heterojunction system is formed by establishing a tailored interface between two semiconductor photocatalysts, utilizing the distinct energy band alignment. This design promotes efficient spatial separation of photo-generated charge pairs, significantly enhancing the photocatalytic activity [114]. For pure $g\text{-C}_3\text{N}_4$, due to the Coulombic effect, photo-generated electrons in the CB are likely to recombine with holes in the VB. However, in $g\text{-C}_3\text{N}_4$ -based Type II heterojunction systems, the CB potential of $g\text{-C}_3\text{N}_4$, typically around -1.1 eV, is lower than that of the second semiconductor. As a result, photoexcited electrons in the CB of $g\text{-C}_3\text{N}_4$ can rapidly migrate to the CB of photocatalyst II, which has a higher potential. Simultaneously, the photo-generated holes shift in the reverse direction. This separation significantly reduces the recombination of electrons and holes, thereby extending their lifetime. Figure 5a schematically illustrates the separation pathway of photo-generated electron–hole pairs in a type-II heterojunction.

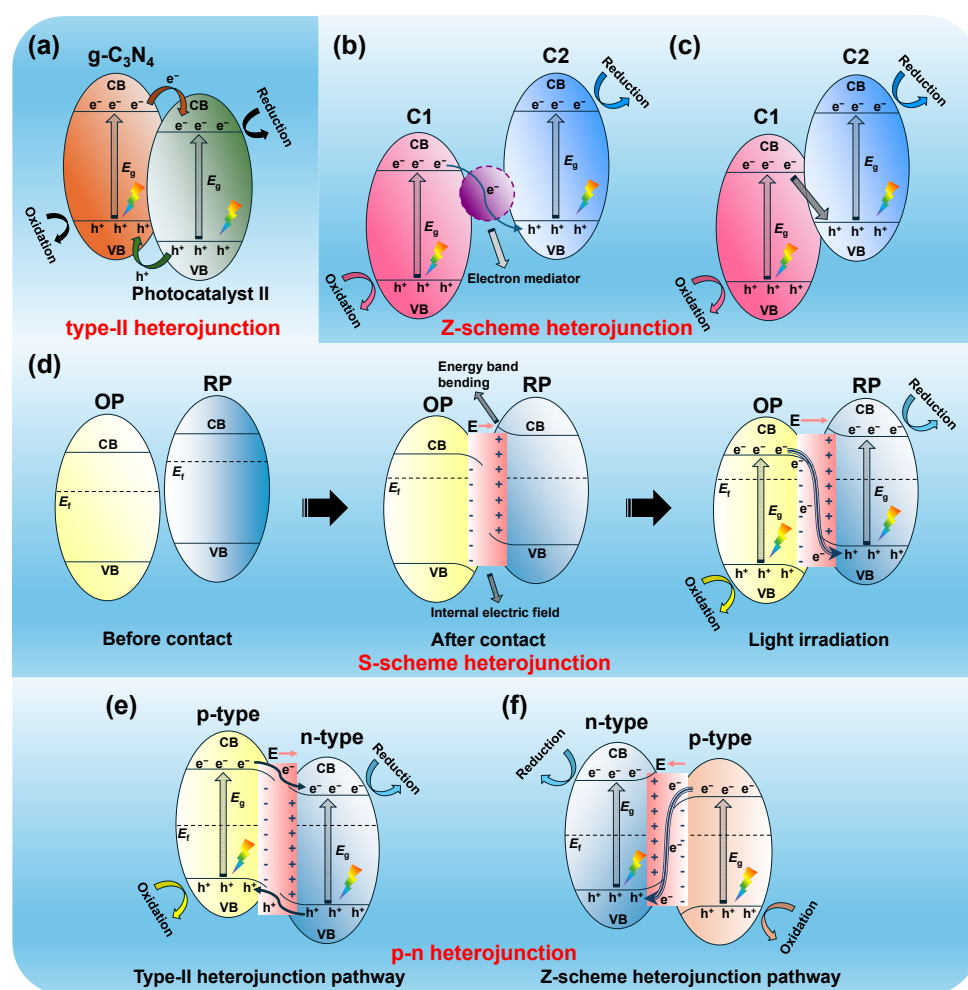


Figure 5. Schematic illustration of the separation pathways of photo-generated electron–hole pairs in a type-II heterojunction (a), a Z-scheme heterojunction with an electron mediator (b), a direct Z-scheme heterojunction (c), an S-scheme heterojunction (d), depicting the band structure before contact, the formation of a built-in electric field and band bending, and the charge transfer pathway under light irradiation, as well as the different charge migration pathways in the p-n heterojunction: type-II heterojunction pathway (e) and Z-scheme heterojunction pathway (f).

To date, various $g\text{-C}_3\text{N}_4$ -based type II heterojunctions have been constructed, exploring different semiconductor materials, including metal oxides (e.g., TiO_2 [115], CeO_2 [116], Fe_2O_3 [117], Cu_2O [118]), metal sulfides (e.g., MoS_2 [119], ZnIn_2S_4 [120], SnS_2 [121]), halides

(e.g., BiOBr [122], BiOI [123]), and other semiconductors (e.g., ZnFe₂O₄ [124], BiVO₄ [125], CoTiO₃ [126], LDH [127], MOFs [128], COFs [129]). Numerous studies have demonstrated that Type-II heterojunctions are effective in promoting the separation of photo-generated charge carriers [130]. For instance, Song et al. [131] fabricated boron-doped carbon dot (BC-dot)-decorated g-C₃N₄ (C₃N₄/BC-dots) photocatalysts through surface deposition. The boron doping treatment transformed the BC-dots from semimetals into semiconductors, leading to the construction of a type II heterojunction between the C₃N₄ and BC-dots, which facilitated the separation of electrons and holes. The experimental data revealed that BC-dots/C₃N₄ possessed a large SSA, fast charge transfer rate, and superior visible light absorption. Additionally, construction of type II heterojunctions also enhances the photoelectrochemical properties of g-C₃N₄ to different extent, depending on the specific characteristics of the second semiconductor material [132].

2.7.2. Z-Scheme Heterojunction

While g-C₃N₄-based Type-II heterojunction photocatalysts enhance photo-generated electron-hole separation, photocatalytic reactions may occur on semiconductors with lower redox potentials, thereby reducing both the reduction and oxidation capability from a thermodynamic standpoint [12,19,114]. A key challenge in designing g-C₃N₄-based heterojunction systems is to efficiently separate photo-generated charge carriers while preserving strong redox properties.

To address these issues, Bard et al. [133] introduced the groundbreaking concept of Z-scheme photocatalytic systems in 1979. Based on the natural photosynthesis process in green plants, this unique charge transfer pathway enhances the separation of electron-hole pairs while maintaining strong redox capability. Figure 5b depicts the typical Z-scheme electron-hole pair transfer mechanism between two semiconductors (C1 and C2), facilitated by electron mediators. In this system, photoexcited electrons in the lower CB of C1 migrate to an electron mediator. The mediator then passes these electrons to the VB of C2, where they recombine with photo-generated holes. This process effectively separates the electron-hole pairs in both semiconductors, with electrons remaining in C2 and holes in C1, thereby enhancing the redox ability of both semiconductors.

A conventional Z-scheme system is usually limited to liquid-phase application due to the necessity of redox mediators. Therefore, the development of all-solid-state Z-scheme photocatalytic systems, where solid conductive materials either replace or eliminate the need for mediators, is highly important [134]. Tada et al. [135] proposed an all-solid-state Z-scheme photocatalyst in 2006, which includes two semiconductors and a solid electron mediator between them. These all-solid-state systems can be employed in a variety of phases, including solutions, gases, and solids, thus broadening their scope of application. However, the solid electron mediators that are required for enhancing electron migration in these systems are often costly and scarce, posing a significant barrier to their large-scale deployment.

Building on previous concepts, Yu et al. [136] presented an innovative idea of direct Z-scheme heterojunctions in 2013. Unlike traditional all-solid-state Z-scheme photocatalysts, which require costly electron mediators, direct Z-scheme photocatalysts eliminate this need, greatly reducing the production cost. In such systems, the electrostatic attraction between photo-generated electrons and holes enhances the charge transfer, making it more efficient than in Type II heterojunctions. Specifically, as shown in Figure 5c, the electrostatic interaction facilitates the transport of electrons from the CB of C1 to the VB of C2, which is rich in holes [134]. Wang et al. [137] constructed a Fe-g-C₃N₄/Bi₂MoO₆ (FCNB) Z-scheme heterojunction enriched with oxygen vacancies. This structure exhibited excellent activity in photocatalytic Fenton degradation of TC under visible light. The introduction of the

Z-scheme heterojunction effectively suppressed the recombination of electron–hole pairs at the interface.

Z-scheme heterojunction systems require the coupling of two semiconductors with appropriate bandgap structures and closely aligned energy bands to achieve favorable charge carrier separation and transfer. This limits the selection of materials for the construction of Z-scheme photocatalysts [138]. Moreover, the complexity of semiconductor interfaces and the high contact resistance could inhibit the transport of charge carriers, leading to inferior photocatalytic activity [139,140]. To mitigate these issues, researchers have constructed dual Z-scheme heterojunction systems, where the combination of multiple components enhances the photon absorption range of photocatalysts [141,142]. Ma et al. [143] synthesized a $g\text{-C}_3\text{N}_4/\text{Bi}_2\text{O}_2\text{CO}_3/\beta\text{-Bi}_2\text{O}_3$ ternary heterojunction via a Bi-based metal–organic framework (Bi-MOF) derivative strategy. This material possessed a high SSA, excellent visible light utilization efficiency, and enhanced charge spatial separation ability due to the electronic transfer pathway via Bi–N bonds and the formation of the heterojunction. Under visible light excitation, approximately 96.7% of TC degraded in the presence of this heterojunction within 120 min, and the reaction rate constant (0.023 min^{-1}) was 4.6 times higher than that of $g\text{-C}_3\text{N}_4$.

2.7.3. S-Scheme Heterojunction

The present Z-scheme heterojunction mechanism has some drawbacks in explaining charge transfer during photocatalysis. In 2019, Yu et al. [144] established a Step-scheme (S-scheme) heterojunction (Figure 5d), which can visually describe the transfer pathway of electrons from lower to higher energy levels, resembling the “steps” of a staircase, thus offering new insights into the charge transfer process in heterojunction photocatalysts [145,146]. This system consists of two specific semiconductors: an oxidation photocatalyst (OP) and a reduction photocatalyst (RP), which can be either n-type or p-type semiconductors. However, the CB position and E_f of the RP must be higher than those of the OP [146]. The contact between the OP and RP causes electrons to migrate from the RP to the OP, driven by the difference in E_f , until an equilibrium is reached. The change in interface charge causes the energy bands of the OP to bend downward, forming an accumulation layer, while the energy bands of the RP bend upward at the interface, resulting in a depletion layer of electrons and creating an internal electric field that promotes the transfer of photo-generated electrons from the OP to the RP. The charge transfer at the interface of the two photocatalysts is driven by the internal electric field that is formed between them [147]. This S-scheme heterojunction effectively enhances charge carrier separation while preserving the redox capability, offering a significant advantage over traditional Type II heterojunctions [114]. Duan et al. [148] fabricated an S-scheme heterojunction photocatalyst by integrating CdS with sulfur-doped carbon nitride (GCNS) using a straight-forward solid-state diffusion technique. The photocatalytic degradation rate constant of methyl orange in the presence of this heterojunction was 9.67 and 5.39 times higher than those of GCNS and CdS, respectively. DFT calculations and charge flow tracking revealed that the S-scheme was formed as a result of the unidirectional band edge bending, which facilitates the migration of electrons from CdS to GCNS. This configuration significantly enhanced the light absorption, improved charge separation, and promoted the generation of $\bullet\text{O}_2^-$ species.

Similar to the dual Z-scheme heterojunctions, $g\text{-C}_3\text{N}_4$ -based dual S-scheme heterojunctions have also been proposed to address the limitations of single-junction S-scheme structures, including weak interactions and poor multiphase integration [147,149]. Zhao et al. [150] reported a dual S-scheme heterojunction, $\text{CeO}_2/g\text{-C}_3\text{N}_4/\text{Bi}_2\text{O}_4$, which exhibited excellent photocatalytic activity and stability. The dual S-scheme electron mi-

gration pathway significantly facilitates the transport of photo-generated charge carriers, suppresses electron–hole recombination, and maintains high redox activity.

2.7.4. p-n Heterojunction

In typical p-type semiconductors, holes are the primary charge carriers, whereas in n-type semiconductors, free electrons serve as the dominant charge carriers. g-C₃N₄, with its –NH/NH₂ groups acting as electron donors, is classified as an n-type semiconductor. Thus, g-C₃N₄ can be coupled with a suitable p-type semiconductor to construct a p-n heterojunction for enhanced photo-generated charge separation [12,151]. Typically, the E_f of p-type semiconductors is close to the VB, while it is near the CB in n-type semiconductors. The contact of these two semiconductors leads to band bending at the interface, forming an internal electric field. This field aids in the transfer of photo-generated electrons from the p-type to the n-type semiconductor, while holes migrate in the reverse direction. This p-n heterojunction structure promotes effective charge separation in g-C₃N₄, enhancing its photocatalytic activity [114].

Interestingly, although the photo-generated electron transfer mechanism in p-n heterojunctions always involves the movement of electrons from the p-type semiconductor to the n-type semiconductor, the pathway of charge carrier transfer can vary significantly owing to the difference in their E_f values. As shown in Figure 5e, if the E_f of the p-type semiconductor is higher than that of the n-type semiconductor, the photo-generated charge carriers will transfer through the Type-II heterojunction path. The presence of built-in electric field accelerates this process. Conversely, photo-generated charge carriers will transfer through the Z-scheme heterojunction path pathway if the E_f of the p-type semiconductor is lower than that of the n-type semiconductor (Figure 5f), driven by the internal electric field. This mode is analogous to the S-scheme heterojunction that is formed between n-type and p-type semiconductors, which efficiently suppresses the recombination of electron–hole pairs while maintaining strong redox capability.

Recent studies have used various p-type semiconductors, including CuAl₂O₄ [152], NiO [153], Mn₃O₄ [154], and BiOI [155], for constructing p-n heterojunctions with g-C₃N₄. Wang et al. [152] developed an S-scheme p-n heterojunction by coupling p-type MnS with n-type protonated g-C₃N₄ (PCN) semiconductors for photocatalytic H₂O₂ production and achieved in situ oxidative degradation of oxytetracycline. The construction of a p-n heterojunction significantly enhanced the photo-generated charge separation and electron transfer efficiency.

3. Oxidant Coupling Strategy to Enhance the Photocatalytic Degradation Efficiency of Organic Pollutants

g-C₃N₄-based photocatalysts have been applied for the photocatalytic degradation of various organic pollutants, such as dyes [156], antibiotics [157], microplastics [158], pharmaceutical and personal care products [159], and pesticides [59]. Various strategies have been adopted to enhance the photocatalytic activity of g-C₃N₄ and performance in pollutant degradation. For instance, Liu et al. [160] developed an innovative Z-scheme heterojunction composed of Ag/AgVO₃ and carbon-rich g-C₃N₄ using a simple hydrothermal calcination method, which exhibited excellent solar-driven photocatalytic activity in the degradation of sulfamethazine. The degradation rate constant for the optimal composite was approximately 13 times higher than that of carbon-rich g-C₃N₄ and 30 times higher than that of Ag/AgVO₃. •O₂[−] was revealed to be the key ROS in the Z-scheme photocatalytic system. Notably, due to the difference in redox potential among different ROSs, the degradation efficiency of organic pollutants depends not only on the rate of ROS generation, but also on the types of ROSs produced. However, most of the ROSs generated under light irradiation

in typical photocatalytic systems of $g\text{-C}_3\text{N}_4$ -based photocatalysts are $\bullet\text{O}_2^-$, which has a relatively weak oxidizing power.

An increasing number of researchers have begun to employ strategies that couple $g\text{-C}_3\text{N}_4$ -based photocatalysts with oxidants to enhance the generation of ROSs, aiming to optimize the photocatalytic degradation efficiency of organic pollutants. Figure 6 briefly summarizes the major oxidants that have been coupled with $g\text{-C}_3\text{N}_4$ -based photocatalysts in the degradation of organic pollutants. Qin et al. [161] fabricated carbon-rich graphitic carbon nitride ($\text{Fe}_1/\text{C-CN}$) containing single-atomic Fe-N_4 sites in the interlayer, which exhibited excellent activity in the degradation of *p*-nitrophenol in the presence of H_2O_2 as an oxidant during the photo-Fenton-like catalytic oxidation process. The pseudo-first-order degradation rate constant of *p*-nitrophenol in the coupled oxidation process was 7.5 times greater than that of $\text{Fe}_1/\text{C-CN}$ photocatalysis and 21.1 times higher than that of Fenton-like system, and complete TOC removal was achieved after 4 h of reaction. The enhanced separation of electron-hole pairs was key in the process, which was coupled with the efficient regeneration of $\equiv\text{Fe(II)}$ and the activation of H_2O_2 on $\text{Fe}_1/\text{C-CN}$. The synergistic effect of these factors greatly enhanced the generation of ROSs, including $\bullet\text{OH}$, $\bullet\text{O}_2^-$, and $^1\text{O}_2$, thereby improving the oxidation of *p*-nitrophenol and its transformation intermediates.

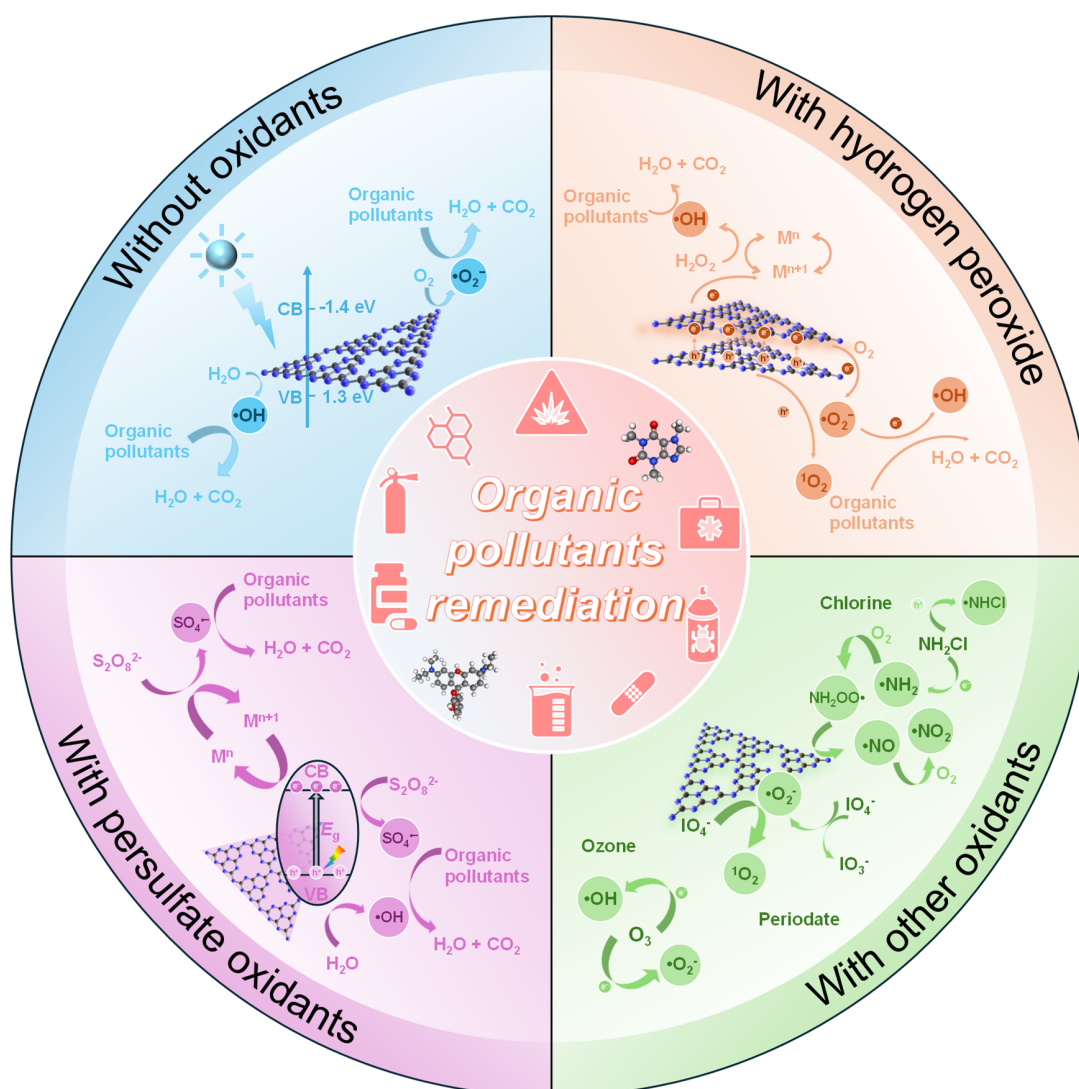


Figure 6. Summary of the major oxidants that have been coupled with $g\text{-C}_3\text{N}_4$ -based photocatalysts in photocatalytic degradation of organic pollutants.

In addition to hydrogen peroxide, photo-assisted AOPs with the addition of persulfate oxidants have also demonstrated superior degradation performance. Nguyen et al. [162] successfully developed a flower-like core-shell heterojunction by integrating manganese dioxide (MnO_2) nanosheets with B and S co-doped $\text{g-C}_3\text{N}_4$ (CNBS) nanotubes to create a Z-scheme CNBS@ MnO_2 photocatalyst. This structure significantly enhanced the photocatalytic degradation of diclofenac (DCF) when combined with peroxymonosulfate (PMS) under visible light (460 nm). Near complete degradation of DCF occurred within just 15 min of light irradiation. The Z-scheme CNBS@ MnO_2 not only facilitates efficient charge carrier separation, but also activates the PMS, generating a range of reactive radicals, such as h^+ , $\bullet\text{O}_2^-$, and $\text{SO}_4^{\bullet-}$, which are responsible for the fast degradation of DCF.

Besides hydrogen peroxide and persulfate, $\text{g-C}_3\text{N}_4$ -based photocatalysts can also be coupled with a range of other oxidants, such as chlorine-containing oxidants [163], ozone [164], periodate (PI) [165], acetylacetone (AA) [166], permanganate [Mn(VII)] [167], and peracetic acid (PAA) [168], to generate different types of ROSs, to enhance the degradation and mineralization of organic pollutants [169]. For instance, Cheng et al. [163] constructed a visible-light-driven $\text{g-C}_3\text{N}_4$ -enabled chlorine advanced oxidation process (VgC-AOP). The pseudo-first-order degradation rate constant of carbamazepine in this process was 16 and 7 times greater than those in the systems without $\text{g-C}_3\text{N}_4$ and HOCl/ClO^- , respectively. Additionally, the VgC-AOP system showed stable performance over multiple use cycles. Unlike traditional HOCl/ClO^- systems, which only produce radicals under UV light, this process successfully expanded the visible light absorption (>400 nm), thereby enhancing its potential in practical application.

Overall, coupling oxidants with $\text{g-C}_3\text{N}_4$ -based photocatalysts to generate multiple highly oxidative ROSs is a promising strategy for enhancing the photocatalytic degradation of pollutants. This approach can be combined with the design strategies of $\text{g-C}_3\text{N}_4$ -based photocatalysts discussed in the above section. Nonetheless, overdosing of oxidants poses a potentially significant problem in practical application, as the generation of excessive ROSs may lead to ROS quenching, thereby impairing the degradation efficiency of targeted pollutants. Thus, the selection of appropriate oxidants and their doses should be tailored based on the type and concentration of organic pollutants to be treated.

4. Conclusions and Perspectives

Photocatalytic degradation of organic pollutants has become one of the most effective techniques for harvesting solar energy for pollution control. $\text{g-C}_3\text{N}_4$, with its low cost, strong visible light absorption, and high stability, is considered a promising non-metal semiconductor photocatalyst. However, the easy recombination of photo-generated charge carriers and the relatively weak redox capability limit its large-scale application. This review systematically summarizes the major strategies for enhancing the photocatalytic activity of $\text{g-C}_3\text{N}_4$ -based photocatalysts, including morphology control, doping, functionalization, metal deposition, dye sensitization, defect engineering, and construction of heterojunctions. The enhanced photocatalytic activity is attributed to the improved charge carrier separation, reduced bandgap, expanded light absorption, and suppressed charge recombination. Additionally, the strategy of coupling oxidants, such as hydrogen peroxide and persulfate, with $\text{g-C}_3\text{N}_4$ -based photocatalysts to enhance the photocatalytic degradation of organic pollutants was also briefly discussed.

Despite the significant progress that has been made through the development of various strategies to enhance the photocatalytic performance of $\text{g-C}_3\text{N}_4$ -based photocatalysts, several critical challenges remain, particularly for their practical application in industrial-scale wastewater treatment.

1. While many strategies have demonstrated significant performance enhancement in laboratory-scale experiments, ensuring long-term stability of the photocatalysts under harsh industrial conditions remains a pressing issue. Photocatalysts often degrade or lose efficiency with prolonged use, especially when exposed to complex wastewater matrices containing various inorganic and organic components. Additionally, the mineralization rates of organic pollutants are often insufficient, requiring further optimization of the photocatalysts' oxidizing capability.
2. The synergistic or antagonistic effects of combining multiple catalyst design strategies remain poorly understood. In-depth understanding of the inter-relationship between these strategies is essential for designing more efficient and cost-effective photocatalysts.
3. Precise control over the structure of g-C₃N₄ during the synthesis process poses a significant challenge. Some of the aforementioned strategies, such as morphology control and construction of heterojunctions, require precise regulation of the surface structure to optimize photocatalytic performance.

Author Contributions: Conceptualization, Writing—original draft preparation, and Writing—review and editing, Y.R.; Conceptualization, Writing—review and editing, Supervision, and Funding acquisition, Y.H.; Conceptualization, Writing—original draft preparation, Writing—review and editing, Supervision, and Funding acquisition, H.C. All authors have read and agreed to the published version of the manuscript.

Funding: This work was partially supported by the Natural Science Foundation of China (Grant Nos. U23A2005, 42477251, and 42277226).

Data Availability Statement: No new data were created or analyzed in this study.

Conflicts of Interest: The authors declare no conflicts of interest.

References

1. Bisaria, K.; Sinha, S.; Singh, R.; Iqbal, H.M.N. Recent advances in structural modifications of photo-catalysts for organic pollutants degradation—A comprehensive review. *Chemosphere* **2021**, *284*, 131263. [[CrossRef](#)] [[PubMed](#)]
2. Kaur, P.K.; Badru, R.; Singh, P.P.; Kaushal, S. Photodegradation of organic pollutants using heterojunctions: A review. *J. Environ. Chem. Eng.* **2020**, *8*, 103666.
3. Li, Z.; Zheng, T.; Li, M.; Liu, X. Organic contaminants in the effluent of Chinese wastewater treatment plants. *Environ. Sci. Pollut. Res.* **2018**, *25*, 26852–26860. [[CrossRef](#)] [[PubMed](#)]
4. Ruan, Y.; Kong, L.; Zhong, Y.; Diao, Z.; Shih, K.; Hou, L.A.; Wang, S.; Chen, D. Review on the synthesis and activity of iron-based catalyst in catalytic oxidation of refractory organic pollutants in wastewater. *J. Clean Prod.* **2021**, *321*, 128924. [[CrossRef](#)]
5. Shanmugavel, S.P.; Kumar, G.; Yogalakshmi, K.N.; Gunasekaran, M.; Banu, J.R. Recent progress in mineralization of emerging contaminants by advanced oxidation process: A review. *Environ. Pollut.* **2024**, *341*, 122842.
6. Huang, S.; Tian, F.; Dai, J.; Tian, X.; Li, G.; Liu, Y.; Chen, Z.; Chen, R. Highly efficient degradation of chlorophenol over bismuth oxides upon near-infrared irradiation: Unraveling the effect of Bi-O-Bi-O defects cluster and 1O₂ involved process. *Appl. Catal. B-Environ.* **2021**, *298*, 120576. [[CrossRef](#)]
7. Zhong, Y.; Shih, K.; Diao, Z.; Song, G.; Su, M.; Hou, L.A.; Chen, D.; Kong, L. Peroxymonosulfate activation through LED-induced ZnFe₂O₄ for levofloxacin degradation. *Chem. Eng. J.* **2021**, *417*, 129225. [[CrossRef](#)]
8. Tan, W.; Ruan, Y.; Diao, Z.; Song, G.; Su, M.; Hou, L.A.; Chen, D.; Kong, L.; Deng, H. Removal of levofloxacin through adsorption and peroxymonosulfate activation using carbothermal reduction synthesized nZVI/carbon fiber. *Chemosphere* **2021**, *280*, 130626. [[CrossRef](#)]
9. Guo, Q.; Zhou, C.; Ma, Z.; Yang, X. Fundamentals of TiO₂ Photocatalysis: Concepts, Mechanisms, and Challenges. *Adv. Mater.* **2019**, *31*, 1901997. [[CrossRef](#)]
10. Schneider, J.; Matsuoka, M.; Takeuchi, M.; Zhang, J.; Horiuchi, Y.; Anpo, M.; Bahnemann, D.W. Understanding TiO₂ Photocatalysis: Mechanisms and Materials. *Chem. Rev.* **2014**, *114*, 9919–9986. [[CrossRef](#)]
11. Tachibana, Y.; Vayssieres, L.; Durrant, J.R. Artificial photosynthesis for solar water-splitting. *Nat. Photonics* **2012**, *6*, 511–518. [[CrossRef](#)]
12. Fu, J.; Yu, J.; Jiang, C.; Cheng, B. g-C₃N₄-Based Heterostructured Photocatalysts. *Adv. Energy Mater.* **2018**, *8*, 1701503. [[CrossRef](#)]

13. Cao, S.; Low, J.; Yu, J.; Jaroniec, M. Polymeric Photocatalysts Based on Graphitic Carbon Nitride. *Adv. Mater.* **2015**, *27*, 2150–2176. [[CrossRef](#)] [[PubMed](#)]
14. Ong, W.; Tan, L.-L.; Ng, Y.H.; Yong, S.; Chai, S. Graphitic Carbon Nitride (g-C₃N₄)-Based Photocatalysts for Artificial Photosynthesis and Environmental Remediation: Are We a Step Closer to Achieving Sustainability? *Chem. Rev.* **2016**, *116*, 7159–7329. [[CrossRef](#)]
15. Guo, R.; Wang, J.; Bi, Z.; Chen, X.; Hu, X.; Pan, W. Recent advances and perspectives of g-C₃N₄-based materials for photocatalytic dyes degradation. *Chemosphere* **2022**, *295*, 133834. [[CrossRef](#)] [[PubMed](#)]
16. Ma, X.; Wang, G.; Qin, L.; Liu, J.; Li, B.; Hu, Y.; Cheng, H. Z-scheme g-C₃N₄-AQ-MoO₃ photocatalyst with unique electron transfer channel and large reduction area for enhanced sunlight photocatalytic hydrogen production. *Appl. Catal. B-Environ. Energy* **2021**, *288*, 120025. [[CrossRef](#)]
17. Ma, X.; Cheng, H. Self-introduction of carbon nitride quantum dots into carbon nitride planar structure for enhanced photocatalytic hydrogen production. *Appl. Catal. B-Environ.* **2023**, *339*, 123101. [[CrossRef](#)]
18. Nemiwal, M.; Zhang, T.C.; Kumar, D. Recent progress in g-C₃N₄, TiO₂ and ZnO based photocatalysts for dye degradation: Strategies to improve photocatalytic activity. *Sci. Total Environ.* **2021**, *767*, 144896. [[CrossRef](#)]
19. Wen, J.; Xie, J.; Chen, X.; Li, X. A review on g-C₃N₄-based photocatalysts. *Appl. Surf. Sci.* **2017**, *391*, 72–123. [[CrossRef](#)]
20. Raaja Rajeshwari, M.; Okla, M.K.; Kokilavani, S.; Abdel-Maksoud, M.A.; Saleh, I.A.; Abu-Harirah, H.A.; AlRamadneh, T.N.; Khan, S.S. Synergistic visible light assisted photocatalytic degradation of *p*-chlorophenol and rifampicin from aqueous solution using a novel g-C₃N₄ quantum dots incorporated alpha-MoO₃ nanohybrid—Mechanism, pathway and toxicity studies. *Chemosphere* **2023**, *339*, 139529. [[CrossRef](#)]
21. Li, C.; Wu, J.; Wang, X.; Cai, Y.; Jia, R.; Wang, W.; Xia, S.; Li, L.; Chen, Z.; Jin, C.-C. One-step preparation of Z-scheme g-C₃N₄ nanorods/TiO₂ microsphere with improved photodegradation of antibiotic residue. *Ceram. Int.* **2024**, *50*, 42127–42134. [[CrossRef](#)]
22. Cui, D.; Yang, X.; Liu, Y.; Ou, T.; Kong, X.; Zhang, Y.; Zhang, J.; Li, F. Strategy of constructing D-A structure and accurate active sites over graphitic carbon nitride nanowires for high efficient photocatalytic nitrogen fixation. *J. Colloid Interface Sci.* **2025**, *678*, 955–969. [[CrossRef](#)] [[PubMed](#)]
23. Liang, D.; Shan, R.; Gu, J.; Wang, S.; Cheng, L.; Yuan, H.; Chen, Y. Unraveling the impact of three coordinate nitrogen (N_{3c}) vacancies in porous carbon nitride nanobelt for boosted photocatalytic degradation of microplastics and antibiotics. *Appl. Catal. B-Environ.* **2024**, *358*, 124402. [[CrossRef](#)]
24. Dai, J.; Liu, Z.; Song, Y.; Liu, Y.; Nghiem, L.D.; Wang, Q.; Liu, W.; Sun, X.; Cai, Z. Heterocyclic polymerization modified g-C₃N₄ nanotube with advanced charge separation for solar light driven degradation of ciprofloxacin. *Sep. Purif. Technol.* **2024**, *348*, 127692. [[CrossRef](#)]
25. Altendji, K.; Hamoudi, S. Efficient Photocatalytic Degradation of Aqueous Atrazine over Graphene-Promoted g-C₃N₄ Nanosheets. *Catalysts* **2023**, *13*, 1265. [[CrossRef](#)]
26. Liang, H.; Zhao, J.; Wang, A.; Kannan, P.; Jing, S.; Chen, F.; Tsiakaras, P. Synthesis of novel nanoflowers-like P, K co-doped graphitic carbon nitride for efficient H₂O₂ photoproduction. *J. Colloid Interface Sci.* **2025**, *677*, 729–739. [[CrossRef](#)] [[PubMed](#)]
27. Sun, G.; Tai, Z.; Zhang, J.; Cheng, B.; Yu, H.; Yu, J. Bifunctional g-C₃N₄ nanospheres/CdZnS QDs S-scheme photocatalyst with boosted H₂ evolution and furfural synthesis mechanism. *Appl. Catal. B-Environ.* **2024**, *358*, 124459. [[CrossRef](#)]
28. Li, Y.; Zhou, B.; Zhang, H.; Huang, T.; Wang, Y.; Huang, W.; Hu, W.; Pan, A.; Fan, X.; Huang, G. A host-guest self-assembly strategy to enhance π -electron densities in ultrathin porous carbon nitride nanocages toward highly efficient hydrogen evolution. *Chem. Eng. J.* **2022**, *430*, 132880. [[CrossRef](#)]
29. Xiao, S.; Yin, R.; Wu, L.; Wu, S.; Tian, G.; Shalom, M.; Wang, L.; Wang, Y.; Pu, F.; Barad, H.; et al. Hierarchically Porous Few-Layer Carbon Nitride and Its High H₂ plus Selectivity for Efficient Photocatalytic Seawater Splitting. *Nano Lett.* **2023**, *23*, 4390–4398. [[CrossRef](#)]
30. Wang, S.; Zhang, J.; Li, B.; Sun, H.; Wang, S.; Duan, X. Morphology-dependent photocatalysis of graphitic carbon nitride for sustainable remediation of aqueous pollutants: A mini review. *J. Environ. Chem. Eng.* **2022**, *10*, 107438. [[CrossRef](#)]
31. Wang, A.; Guo, S.; Zheng, Z.; Wang, H.; Song, X.; Zhu, H.; Zeng, Y.; Lam, J.; Qiu, R.; Yan, K. Highly dispersed Ag and g-C₃N₄ quantum dots co-decorated 3D hierarchical Fe₃O₄ hollow microspheres for solar-light-driven pharmaceutical pollutants degradation in natural water matrix. *J. Hazard. Mater.* **2022**, *434*, 128905. [[CrossRef](#)] [[PubMed](#)]
32. Tian, N.; Huang, H.; Du, X.; Dong, F.; Zhang, Y. Rational nanostructure design of graphitic carbon nitride for photocatalytic applications. *J. Mater. Chem. A* **2019**, *7*, 11584–11612. [[CrossRef](#)]
33. Zhang, X.; Li, X.; Yu, P.; Yu, Y.; Fan, X.; Zhang, J.; Yu, Y.; Zheng, H.; Sun, Y. Photocatalytic O₂ activation by metal-free carbon nitride nanotube for rapid reactive species generation and organic contaminants degradation. *J. Hazard. Mater.* **2023**, *456*, 131715. [[CrossRef](#)] [[PubMed](#)]
34. Chen, L.; Maigbay, M.A.; Li, M.; Qiu, X. Synthesis and modification strategies of g-C₃N₄ nanosheets for photocatalytic applications. *Adv. Powder Mater.* **2024**, *3*, 100150. [[CrossRef](#)]

35. Panneri, S.; Ganguly, P.; Mohan, M.; Nair, B.N.; Mohamed, A.A.P.; Warriar, K.G.; Hareesh, U.S. Photoregenerable, Bifunctional Granules of Carbon-Doped g-C₃N₄ as Adsorptive Photocatalyst for the Efficient Removal of Tetracycline Antibiotic. *ACS Sustain. Chem. Eng.* **2017**, *5*, 1610–1618. [[CrossRef](#)]
36. Huang, Y.; Li, D.; Feng, S.; Jia, Y.; Guo, S.; Wu, X.; Chen, M.; Shi, W. Pt Atoms/Clusters on Ni-phytate-sensitized Carbon Nitride for Enhanced NIR-light-driven Overall Water Splitting beyond 800 nm. *Angew. Chem.-Int. Edit.* **2022**, *61*, e202212234. [[CrossRef](#)]
37. Kuate, L.J.N.; Chen, Z.; Lu, J.; Wen, H.; Guo, F.; Shi, W. Photothermal-Assisted Photocatalytic Degradation of Tetracycline in Seawater Based on the Black g-C₃N₄ Nanosheets with Cyano Group Defects. *Catalysts* **2023**, *13*, 1147. [[CrossRef](#)]
38. Nguyen, T.; Sherpa, K.; Chen, C.; Chen, L.; Thao Ho, P.N.; Dong, C. Enhancing photocatalytic reduction of Cr(VI) in water through morphological manipulation of g-C₃N₄ photocatalysts: A comparative study of 1D, 2D, and 3D structures. *Chemosphere* **2024**, *362*, 142787. [[CrossRef](#)]
39. Gnanaguru, M.V.L.; Dey, D.; Ghangrekar, M.M.; Sen, R.; Chowdhury, S. 3D g-C₃N₄/WS₂/Agarose Aerogel Photocatalyst for Near-Complete Degradation of Broad-Spectrum Antibiotics in Batch and Continuous Flow Modes. *ACS EST Eng.* **2024**. [[CrossRef](#)]
40. Tian, N.; Xiao, K.; Zhang, Y.; Lu, X.; Ye, L.; Gao, P.; Ma, T.; Huang, H. Reactive sites rich porous tubular yolk-shell g-C₃N₄ via precursor recrystallization mediated microstructure engineering for photoreduction. *Appl. Catal. B-Environ.* **2019**, *253*, 196–205. [[CrossRef](#)]
41. Yu, Y.; Huang, H. Coupled adsorption and photocatalysis of g-C₃N₄ based composites: Material synthesis, mechanism, and environmental applications. *Chem. Eng. J.* **2023**, *453*, 139755. [[CrossRef](#)]
42. Bhagat, B.R.; Dashora, A. Understanding the synergistic effect of Co-loading and B-doping in g-C₃N₄ for enhanced photocatalytic activity for overall solar water splitting. *Carbon* **2021**, *178*, 666–677. [[CrossRef](#)]
43. Lu, W.; Wang, A.; Zhang, Y.; Ren, S.; Zhang, Z. Insights into enhanced degradation of antibiotic trimethoprim in water using a novel K doped g-C₃N₄ photocatalyst under vacuum-UV irradiation: Performance and mechanisms. *Chem. Eng. J.* **2024**, *495*, 153192. [[CrossRef](#)]
44. Zhou, Z.; Zeng, H.; Li, L.; Tang, R.; Feng, C.; Gong, D.; Huang, Y.; Deng, Y. Methyl contributes to the directed phosphorus doping of g-C₃N₄: pH-dependent selective reactive oxygen species enable customized degradation of organic pollutants. *Water Res.* **2024**, *255*, 121521. [[CrossRef](#)]
45. Bai, Y.; Hu, X.; Tian, T.; Cai, B.; Li, Y. Carbon pre-protected iron strategy to construct Fe, C-codoped g-C₃N₄ for effective photodegradation of organic pollutants via hole oxidation mechanism. *J. Clean Prod.* **2024**, *437*, 140739. [[CrossRef](#)]
46. Niu, B.; Xiao, J.; Xu, Z. Recycling Spent LiCoO₂ Battery as a High-efficient Lithium-doped Graphitic Carbon Nitride/Co₃O₄ Composite Photocatalyst and Its Synergistic Photocatalytic Mechanism. *Energy Environ. Mater.* **2023**, *6*, e12312. [[CrossRef](#)]
47. Liu, Z.; Ruan, Z.; Yang, X.; Huang, Y.; Xing, J. Enhancing Performance of Organic Pollutant Degradation via Building Heterojunctions with ZnO Nanowires and Na Doped Conjugated 2,4,6-Triaminopyrimidin-g-C₃N₄. *Molecules* **2024**, *29*, 3240. [[CrossRef](#)]
48. Yan, W.; Yan, L.; Jing, C. Impact of doped metals on urea-derived g-C₃N₄ for photocatalytic degradation of antibiotics: Structure, photoactivity and degradation mechanisms. *Appl. Catal. B-Environ.* **2019**, *244*, 475–485. [[CrossRef](#)]
49. Lee, Y.-J.; Jeong, Y.J.; Cho, I.S.; Park, S.-J.; Lee, C.-G.; Alvarez, P.J.J. Facile synthesis of N vacancy g-C₃N₄ using Mg-induced defect on the amine groups for enhanced photocatalytic •OH generation. *J. Hazard. Mater.* **2023**, *449*, 131046. [[CrossRef](#)]
50. Nguyen Van, M.; Mai, O.L.; Pham Do, C.; Lam Thi, H.; Pham Manh, C.; Nguyen Manh, H.; Pham Thi, D.; Do Danh, B. Fe-Doped g-C₃N₄: High-Performance Photocatalysts in Rhodamine B Decomposition. *Polymers* **2020**, *12*, 1963. [[CrossRef](#)]
51. Yang, X.; Tian, Z.; Chen, Y.; Huang, H.; Hu, J.; Wen, B. In situ synthesis of 2D ultrathin cobalt doped g-C₃N₄ nanosheets enhances photocatalytic performance by accelerating charge transfer. *J. Alloys Compd.* **2021**, *859*, 157754. [[CrossRef](#)]
52. Nguyen, O.T.K.; Nguyen, V.H.; Nong, L.X.; Doan, Q.-M.T.; Hoang, L.-A.T.; Nam, K.H.; Lee, T.; Nguyen, T.D. Transition metal nickel nanoparticle-decorated g-C₃N₄ photocatalyst for improving tetracycline hydrochloride degradation. *J. Photochem. Photobiol. A-Chem.* **2025**, *459*, 116042. [[CrossRef](#)]
53. Lv, Z.; Feng, J.; Zhao, R.; Shen, J.; Yang, W. Visible-light-driven photocatalytic degradation of ibuprofen by Cu-doped tubular C₃N₄: Mechanisms, degradation pathway and DFT calculation. *Chemosphere* **2024**, *358*, 142106. [[CrossRef](#)] [[PubMed](#)]
54. Kong, Y.; Li, D.; Zhang, C.; Han, W.; Xue, Y.; Zhang, W.; Sun, H.; Wang, S.; Duan, X. Synergistic silver doping and N vacancy promoting photocatalytic performances of carbon nitride for pollutant oxidation and hydrogen production. *Chem. Eng. J.* **2024**, *479*, 147676. [[CrossRef](#)]
55. Jing, M.; Zhao, H.; Jian, L.; Pan, C.; Dong, Y.; Zhu, Y. Coral-like B-doped g-C₃N₄ with enhanced molecular dipole to boost photocatalysis-self-Fenton removal of persistent organic pollutants. *J. Hazard. Mater.* **2023**, *449*, 131017. [[CrossRef](#)]
56. Li, T.; Zhang, X.; Hu, C.; Li, X.; Zhang, P.; Chen, Z. Porous carbon-doped g-C₃N₄ with tunable band structure for boosting photocatalytic H₂O₂ production with simultaneous pollutants removal. *J. Environ. Chem. Eng.* **2022**, *10*, 107116. [[CrossRef](#)]
57. Zeng, Y.; Liu, X.; Liu, C.; Wang, L.; Xia, Y.; Zhang, S.; Luo, S.; Pei, Y. Scalable one-step production of porous oxygen-doped g-C₃N₄ nanorods with effective electron separation for excellent visible-light photocatalytic activity. *Appl. Catal. B-Environ.* **2018**, *224*, 1–9. [[CrossRef](#)]

58. Xing, J.; Huang, X.; Yong, X.; Li, X.; Li, J.; Wang, J.; Wang, N.; Hao, H. N-doped synergistic porous thin-walled g-C₃N₄ nanotubes for efficient tetracycline photodegradation. *Chem. Eng. J.* **2023**, *455*, 140570. [[CrossRef](#)]
59. Zheng, A.; Xie, S.; Li, K.; Zhang, C.; Shi, H. Performance and mechanism investigation on the enhanced photocatalytic removal of atrazine on S-doped g-C₃N₄. *Chemosphere* **2024**, *347*, 140663. [[CrossRef](#)]
60. Bi, L.; Fu, G.; Cai, D.; Shen, J.; Zhang, J.; Kang, J.; Cheng, Y.; Yan, P.; Zhou, Y.; Chen, Z. Electron rich P doped g-C₃N₄ for photodegradation of 2,4-dichlorophenoxyacetic acid under visible light by improving oxygen adsorption: Performance and catalytic mechanism. *Sep. Purif. Technol.* **2023**, *306*, 122562. [[CrossRef](#)]
61. Phoon, B.L.; Yang, T.C.K.; Leo, B.F.; Lai, C.W.; Phang, S.W.; Juan, J.C. Mesoporous semi-ionic F-doped g-C₃N₄ as efficient photocatalyst for tetracycline removal under visible light. *Environ. Technol. Innov.* **2023**, *32*, 103303. [[CrossRef](#)]
62. Guo, F.; Li, M.; Ren, H.; Huang, X.; Shu, K.; Shi, W.; Lu, C. Facile bottom-up preparation of Cl-doped porous g-C₃N₄ nanosheets for enhanced photocatalytic degradation of tetracycline under visible light. *Sep. Purif. Technol.* **2019**, *228*, 115770. [[CrossRef](#)]
63. Hong, J.; Hwang, D.K.; Selvaraj, R.; Kim, Y. Facile synthesis of Br-doped g-C₃N₄ nanosheets via one-step exfoliation using ammonium bromide for photodegradation of oxytetracycline antibiotics. *J. Ind. Eng. Chem.* **2019**, *79*, 473–481. [[CrossRef](#)]
64. Phoon, B.L.; Lai, C.W.; Chen, C.; Boonyuen, S.; Tang, W.K.; Juan, J.C. Mesoporous I-doped-g-C₃N₄ with C vacancies as superior visible-light-driven photocatalyst for removal of tetracycline antibiotic. *J. Alloys Compd.* **2024**, *1009*, 176772. [[CrossRef](#)]
65. Duan, Y.; Li, J.; Jia, D.; Yao, H.; Shang, X.; Li, C. One-step synthesis of Mg-doped g-C₃N₄ nanosheets for efficient photo-Fenton-like catalysis. *Diamond Relat. Mater.* **2022**, *129*, 109313. [[CrossRef](#)]
66. Mao, H.; Wang, L.; Zhang, Q.; Chen, F.; Song, Y.; Gui, H.; Cui, A.; Yao, C. Synergetic Adsorption-Photocatalytic Activated Fenton System via Iron-Doped g-C₃N₄/GO Hybrid for Complex Wastewater. *Catalysts* **2023**, *13*, 88. [[CrossRef](#)]
67. Xie, M.; Tang, J.; Kong, L.; Lu, W.; Natarajan, V.; Zhu, F.; Zhan, J. Cobalt doped g-C₃N₄ activation of peroxymonosulfate for monochlorophenols degradation. *Chem. Eng. J.* **2019**, *360*, 1213–1222. [[CrossRef](#)]
68. Song, T.; Zhang, X.; Xie, C.; Yang, P. N-doped carbon nanotubes enhanced charge transport between Ni nanoparticles and g-C₃N₄ nanosheets for photocatalytic H₂ generation and 4-nitrophenol removal. *Carbon* **2023**, *210*, 118052. [[CrossRef](#)]
69. Bao, J.; Bai, W.; Wu, M.; Gong, W.; Yu, Y.; Zheng, K.; Liu, L. Template-mediated copper doped porous g-C₃N₄ for efficient photodegradation of antibiotic contaminants. *Chemosphere* **2022**, *293*, 133607. [[CrossRef](#)]
70. Ma, S.; Zhan, S.; Jia, Y.; Shi, Q.; Zhou, Q. Enhanced disinfection application of Ag-modified g-C₃N₄ composite under visible light. *Appl. Catal. B-Environ.* **2016**, *186*, 77–87. [[CrossRef](#)]
71. Meng, Y.; Li, Z.; Tan, J.; Li, J.; Wu, J.; Zhang, T.; Wang, X. Oxygen-doped porous graphitic carbon nitride in photocatalytic peroxymonosulfate activation for enhanced carbamazepine removal: Performance, influence factors and mechanisms. *Chem. Eng. J.* **2022**, *429*, 130860. [[CrossRef](#)]
72. Yue, J.; Yang, H.; Zhou, L.; Liu, C.; Wang, S.; Kang, X. At least five: Benefit origins of potassium and sodium co-doping on carbon nitride for integrating pharmaceuticals degradation and hydrogen peroxide production. *Appl. Catal. B-Environ. Energy* **2025**, *361*, 124599. [[CrossRef](#)]
73. Zhang, P.; Cao, X.; Gu, L.; Yu, H.; Wu, F.; Liu, Y.; Liu, X.; Gao, Y.; Zhang, H. Embedded iron and nitrogen co-doped carbon quantum dots within g-C₃N₄ as an exceptional PMS photocatalytic activator for sulfamethoxazole degradation: The key role of Fe-N bridge. *Sep. Purif. Technol.* **2024**, *342*, 126975. [[CrossRef](#)]
74. Deng, X.; Yang, H.; Zhao, D.; Guan, J.; Gu, Z.; Zhang, L. Mn-Cu co-doped graphitic carbon nitride accelerates permonosulfate to generate more singlet oxygen in pollutant degradation. *J. Water Process. Eng.* **2024**, *64*, 105755. [[CrossRef](#)]
75. Wang, N.; Cheng, L.; Liao, Y.; Xiang, Q. Effect of Functional Group Modifications on the Photocatalytic Performance of g-C₃N₄. *Small* **2023**, *19*, 2300109. [[CrossRef](#)]
76. Zhou, C.; Almatrafi, E.; Tang, X.; Shao, B.; Xia, W.; Song, B.; Xiong, W.; Wang, W.; Guo, H.; Chen, S.; et al. Investigation on the structure-performance of phthalic acid carboxyl position and carbon nitride towards efficient photocatalytic degradation of organic pollutants. *Sep. Purif. Technol.* **2022**, *286*, 120464. [[CrossRef](#)]
77. Ma, X.; Cheng, H. In-plane electric field induced by cyano groups and graphitic carbon structure for enhancing photocatalytic hydrogen production of carbon nitride. *Sep. Purif. Technol.* **2024**, *330*, 125260. [[CrossRef](#)]
78. Wang, H.; Xu, X.; Labidi, A.; Ren, H.; Allam, A.A.; Rady, A.; Huang, Y.; Wei, S.; Padervand, M.; Ghasemi, S.; et al. Cyano/Hydroxyl Groups Co-Functionalized g-C₃N₄ for Photocatalytic NO Removal: A Synergistic Strategy towards Inhibition of Toxic Intermediate NO₂. *Catalysts* **2023**, *13*, 1433. [[CrossRef](#)]
79. Wang, C.; Li, H.; Guo, Y.; Zhao, H.; Dong, Y.; Zhu, Y. Efficient Photocatalytic Selective Oxidation of Benzylamines over Cobalt Molecular Catalyst Covalently Bonded to Carboxyl Functionalized Carbon Nitride. *Adv. Energy Sustain. Res.* **2023**, *4*, 2300114. [[CrossRef](#)]
80. Ming, L.; Yue, H.; Xu, L.; Chen, F. Hydrothermal synthesis of oxidized g-C₃N₄ and its regulation of photocatalytic activity. *J. Mater. Chem. A* **2014**, *2*, 19145–19149. [[CrossRef](#)]
81. Xu, M.; Wang, R.; Fu, H.; Shi, Y.; Ling, L. Harmonizing the cyano- group and Na to enhance selective photocatalytic O₂ activation on carbon nitride for refractory pollutant degradation. *Proc. Natl. Acad. Sci. USA* **2024**, *121*, e2318787121. [[CrossRef](#)] [[PubMed](#)]

82. Wang, K.; Li, Y.; Sun, T.; Xue, B. Cyano and terminal amino group co-modified polymeric carbon nitride with boosted photocatalytic activity for degradation of dyes and antibiotics. *Mater. Lett.* **2020**, *277*, 128315. [[CrossRef](#)]
83. Xing, W.; Zhang, T.; Shao, W.; Zhang, Y.; Li, P.; Han, J.; Wu, G.; Chen, G. Boosting surface charge transfer by aldehyde group grafted on loofah-sponge-like carbon nitride for visible light H₂ evolution. *Appl. Surf. Sci.* **2023**, *609*, 155227. [[CrossRef](#)]
84. Yu, K.; Li, Y.; Cao, X.; Wang, R.; Zhou, L.; Wu, L.; He, N.; Lei, J.; Fu, D.; Chen, T.; et al. In-situ constructing amidoxime groups on metal-free g-C₃N₄ to enhance chemisorption, light absorption, and carrier separation for efficient photo-assisted uranium(VI) extraction. *J. Hazard. Mater.* **2023**, *460*, 132356. [[CrossRef](#)]
85. Majdoub, M.; Anfar, Z.; Amedlous, A. Emerging Chemical Functionalization of g-C₃N₄: Covalent/Noncovalent Modifications and Applications. *ACS Nano* **2020**, *14*, 12390–12469. [[CrossRef](#)]
86. Chen, D.; Wang, K.; Hong, W.; Zong, R.; Yao, W.; Zhu, Y. Visible light photoactivity enhancement via CuTCPP hybridized g-C₃N₄ nanocomposite. *Appl. Catal. B-Environ.* **2015**, *166–167*, 366–373. [[CrossRef](#)]
87. Hou, Y.; Cui, C.; Zhang, E.; Wang, J.; Li, Y.; Zhang, Y.; Zhang, Y.; Wang, Q.; Jiang, J. A hybrid of g-C₃N₄ and porphyrin-based covalent organic frameworks via liquid-assisted grinding for enhanced visible-light-driven photoactivity. *Dalton Trans.* **2019**, *48*, 14989–14995. [[CrossRef](#)]
88. Xing, J.; Wang, N.; Li, X.; Wang, J.; Taiwaikuli, M.; Huang, X.; Wang, T.; Zhou, L.; Hao, H. Synthesis and modifications of g-C₃N₄-based materials and their applications in wastewater pollutants removal. *J. Environ. Chem. Eng.* **2022**, *10*, 108782. [[CrossRef](#)]
89. Liu, K.; Wang, X.; Li, C.; Gao, M.; Cao, N.; Zhao, X.; Li, W.; Ding, X.; Li, Z.; Du, X.; et al. Facile fabrication metal Cu-decorated g-C₃N₄ photocatalyst with Schottky barrier for efficient pollutant elimination. *Diamond Relat. Mater.* **2022**, *126*, 109116. [[CrossRef](#)]
90. Chen, M.; Guo, C.; Hou, S.; Wu, L.; Lv, J.; Hu, C.; Zhang, Y.; Xu, J. In-situ fabrication of Ag/P-g-C₃N₄ composites with enhanced photocatalytic activity for sulfamethoxazole degradation. *J. Hazard. Mater.* **2019**, *366*, 219–228. [[CrossRef](#)]
91. Shi, Y.; Li, L.; Xu, Z.; Guo, F.; Li, Y.; Shi, W. Synergistic coupling of piezoelectric and plasmonic effects regulates the Schottky barrier in Ag nanoparticles/ultrathin g-C₃N₄ nanosheets heterostructure to enhance the photocatalytic activity. *Appl. Surf. Sci.* **2023**, *616*, 156466. [[CrossRef](#)]
92. Xin, S.; Ma, X.; Lu, J.; Zhang, G.; Huo, S.; Gao, M.; Xu, P.; Liu, W.; Fu, W. Enhanced visible light photoelectrocatalytic degradation of o-chloronitrobenzene through surface plasmonic Au nanoparticles and g-C₃N₄ co-modified TiO₂ nanotube arrays photoanode. *Appl. Catal. B-Environ. Energy* **2023**, *323*, 122174. [[CrossRef](#)]
93. Xiao, Y.; Li, H.; Yao, B.; Xiao, K.; Wang, Y. Hollow g-C₃N₄@Ag₃PO₄ Core-Shell Nanoreactor Loaded with Au Nanoparticles: Boosting Photothermal Catalysis in Confined Space. *Small* **2024**, *20*, 2308032. [[CrossRef](#)] [[PubMed](#)]
94. He, X.; Wang, L.; Sun, S.; Guo, X.; Tian, H.; Xia, Z.; Li, X.; Yan, X.; Jiao, Z. Photodeposition synthesis of hollow g-C₃N₄/Ag nanotubes with high oxidation properties to enhance visible-light photocatalytic performance. *Mater. Res. Bull.* **2024**, *172*, 112658. [[CrossRef](#)]
95. Huang, Z.; Cai, X.; Zang, S.; Li, Y.; Zheng, D.; Li, F. Strong Metal Support Effect of Pt/g-C₃N₄ Photocatalysts for Boosting Photothermal Synergistic Degradation of Benzene. *Int. J. Mol. Sci.* **2023**, *24*, 6872. [[CrossRef](#)]
96. Lei, M.; Wang, Z.; Zhu, L.; Nie, W.; Tang, H. Complete debromination of 2,2',4,4'-tetrabromodiphenyl ether by visible-light photocatalysis on g-C₃N₄ supported Pd. *Appl. Catal. B-Environ.* **2020**, *261*, 118236. [[CrossRef](#)]
97. Jin, L.; Tanzeel, Q.; Arif, U.; Ali, F.; Ali, N.; Haotian, C.; Mehmood, S.; Akbar, Y.; Raziq, F. Efficient photodegradation of organic dyes from industrial wastewater using novel Ni-decorated g-C₃N₄-TiO₂ photocatalysts. *Colloid Polym. Sci.* **2024**, *302*, 487–502. [[CrossRef](#)]
98. Gawande, M.B.; Goswami, A.; Felpin, F.-X.; Asefa, T.; Huang, X.; Silva, R.; Zou, X.; Zboril, R.; Varma, R.S. Cu and Cu-Based Nanoparticles: Synthesis and Applications in Review Catalysis. *Chem. Rev.* **2016**, *116*, 3722–3811. [[CrossRef](#)]
99. Li, N.; Gao, H.; Wang, X.; Zhao, S.; Lv, D.; Yang, G.; Gao, X.; Fan, H.; Gao, Y.; Ge, L. Novel indirect Z-scheme g-C₃N₄/Bi₂MoO₆/Bi hollow microsphere heterojunctions with SPR-promoted visible absorption and highly enhanced photocatalytic performance. *Chin. J. Catal.* **2020**, *41*, 426–434. [[CrossRef](#)]
100. Li, R.; Wang, X.; Chen, M. Non-Noble Metal and Nonmetallic Plasmonic Nanomaterials with Located Surface Plasmon Resonance Effects: Photocatalytic Performance and Applications. *Catalysts* **2023**, *13*, 940. [[CrossRef](#)]
101. Gonuguntla, S.; Kamesh, R.; Pal, U.; Chatterjee, D. Dye sensitization of TiO₂ relevant to photocatalytic hydrogen generation: Current research trends and prospects. *J. Photochem. Photobiol. C-Photochem. Rev.* **2023**, *57*, 100621. [[CrossRef](#)]
102. Zhang, N.; Wen, L.; Yan, J.; Liu, Y. Dye-sensitized graphitic carbon nitride (g-C₃N₄) for photocatalysis: A brief review. *Chem. Pap.* **2020**, *74*, 389–406. [[CrossRef](#)]
103. Bakhtiar, S.U.H.; Zada, A.; Raziq, F.; Ali, S.; Shah, M.I.A.; Ateeq, M.; Khan, M.; Alei, D.; Fazil, P.; Naeem, M.; et al. Zinc phthalocyanine sensitized g-C₃N₄ photocatalyst for exceptional photocatalytic hydrogen evolution and pollutant degradation. *Int. J. Hydrogen Energy* **2023**, *48*, 16320–16329. [[CrossRef](#)]
104. Zhou, Z.; Zhang, Y.; Shen, Y.; Liu, S.; Zhang, Y. Molecular engineering of polymeric carbon nitride: Advancing applications from photocatalysis to biosensing and more. *Chem. Soc. Rev.* **2018**, *47*, 2298–2321. [[CrossRef](#)] [[PubMed](#)]

105. Jiang, L.; Yang, J.; Yuan, X.; Guo, J.; Liang, J.; Tang, W.; Chen, Y.; Li, X.; Wang, H.; Chu, W. Defect engineering in polymeric carbon nitride photocatalyst: Synthesis, properties and characterizations. *Adv. Colloid Interface Sci.* **2021**, *296*, 102523. [[CrossRef](#)]
106. Li, X.; Wang, G.; Lan, C.; Dong, X.; Zhang, X. New insight into enhanced photocatalytic selectivity of g-C₃N₄ by nitrogen vacancy introduction: Experimental study and theoretical calculation. *Environ. Res.* **2022**, *212*, 113390.
107. Li, Y.; Gu, M.; Shi, T.; Cui, W.; Zhang, X.; Dong, F.; Cheng, J.; Fan, J.; Lv, K. Carbon vacancy in C₃N₄ nanotube: Electronic structure, photocatalysis mechanism and highly enhanced activity. *Appl. Catal. B-Environ.* **2020**, *262*, 118281. [[CrossRef](#)]
108. Song, X.; Yang, Q.; Jiang, X.; Yin, M.; Zhou, L. Porous graphitic carbon nitride nanosheets prepared under self-producing atmosphere for highly improved photocatalytic activity. *Appl. Catal. B-Environ.* **2017**, *217*, 322–330. [[CrossRef](#)]
109. Liu, Q.; Cui, K.; Cui, M.; Liu, X.; Zhang, Q. Co-modification of carbon and cyano defect in g-C₃N₄ for enhanced photocatalytic peroxydisulfate activation: Combined experimental and theoretical analysis. *Sep. Purif. Technol.* **2023**, *316*, 123844. [[CrossRef](#)]
110. Ma, Z.; Ma, X.; Zhang, L.; Cheng, H.; Shi, F.-N. 1T-WS₂/NCN photocatalyst with unique trion behavior and cyano-defects: Photocatalytic hydrogen evolution and mechanistic insights. *Sep. Purif. Technol.* **2023**, *325*, 124743. [[CrossRef](#)]
111. Bai, S.; Zhang, N.; Gao, C.; Xiong, Y. Defect engineering in photocatalytic materials. *Nano Energy* **2018**, *53*, 296–336. [[CrossRef](#)]
112. Li, R.; Zheng, M.; Zhou, X.; Zhang, D.; Shi, Y.; Li, C.; Yang, M. Carbon vacancies in porous g-C₃N₄ nanosheets induced robust H₂O₂ production for highly efficient photocatalysis-self-Fenton system for metronidazole degradation. *Chem. Eng. J.* **2023**, *464*, 142584. [[CrossRef](#)]
113. Liu, Y.; Chen, X.; Kamali, M.; Rossi, B.; Appels, L.; Dewil, R. Unraveling the Presence and Positions of Nitrogen Defects in Defective g-C₃N₄ for Improved Organic Photocatalytic Degradation: Insights from Experiments and Theoretical Calculations. *Adv. Funct. Mater.* **2024**, *34*, 2405741. [[CrossRef](#)]
114. Li, Y.; Zhou, M.; Cheng, B.; Shao, Y. Recent advances in g-C₃N₄-based heterojunction photocatalysts. *J. Mater. Sci. Technol.* **2020**, *56*, 1–17. [[CrossRef](#)]
115. Yadav, S.M.; Desai, M.A.; Sartale, S.D. Superoxide ($\bullet\text{O}_2^-$) radical species driven type II TiO₂/g-C₃N₄ heterojunction photocatalyst for RhB dye degradation. *J. Mater. Sci.-Mater. Electron.* **2023**, *34*, 1651. [[CrossRef](#)]
116. Ma, R.; Zhang, S.; Li, L.; Gu, P.; Wen, T.; Khan, A.; Li, S.; Li, B.; Wang, S.; Wang, X. Enhanced Visible-Light-Induced Photoactivity of Type-II CeO₂/g-C₃N₄ Nanosheet toward Organic Pollutants Degradation. *ACS Sustain. Chem. Eng.* **2019**, *7*, 9699–9708. [[CrossRef](#)]
117. Ge, F.; Li, X.; Wu, M.; Ding, H.; Li, X. A type II heterojunction $\alpha\text{-Fe}_2\text{O}_3$ /g-C₃N₄ for the heterogeneous photo-Fenton degradation of phenol. *RSC Adv.* **2022**, *12*, 8300–8309. [[CrossRef](#)]
118. Mehtab, A.; Mao, Y.; Alshehri, S.M.; Ahmad, T. Photo/electrocatalytic hydrogen evolution using Type-II Cu₂O/g-C₃N₄ Heterostructure: Density functional theory addresses the improved charge transport efficiency. *J. Colloid Interface Sci.* **2023**, *652*, 1467–1480. [[CrossRef](#)]
119. Raj, M.G.; Vijayakumar, E.; Preetha, R.; Narendran, M.G.; Jennifer, G.A.; Varathan, E.; Neppolian, B.; Ganesh, V.K.; Bosco, A.J. Experimental investigation into the π -conjugated HT-g-C₃N₄/MoS₂ (X) evokes the electron transport in type-II heterojunction to achieve high photocatalytic antibiotic removal under visible-light irradiation. *Sep. Purif. Technol.* **2022**, *292*, 121028.
120. Wang, Y.; Li, J.; Chen, S.; Xie, Y.; Ma, Y.; Luo, Y.; Huang, J.; Ling, Y.; Ye, J.; Liang, Y.; et al. In situ loading of ZnIn₂S₄ nanosheets onto S doped g-C₃N₄ nanosheets to construct type II heterojunctions for improving photocatalytic hydrogen production. *J. Alloys Compd.* **2022**, *924*, 166569. [[CrossRef](#)]
121. Wang, H.; Liu, Z.; Wang, L.; Shou, Q.; Gao, M.; Wang, H.; Nazir, A.; Huo, P. Fabrication of g-C₃N₄/SnS₂ type-II heterojunction for efficient photocatalytic conversion of CO₂. *J. Mater. Sci.-Mater. Electron.* **2023**, *34*, 350. [[CrossRef](#)]
122. Vinoth, S.; Pandikumar, A. Ni integrated S-gC₃N₄/BiOBr based Type-II heterojunction as a durable catalyst for photoelectrochemical water splitting. *Renew. Energy* **2021**, *173*, 507–519. [[CrossRef](#)]
123. Vinoth, S.; Rajaiatha, P.M.; Pandikumar, A. Modulating photoelectrochemical water splitting performance by constructing a type-II heterojunction between g-C₃N₄ and BiOI. *New J. Chem.* **2021**, *45*, 2010–2018. [[CrossRef](#)]
124. Shi, Y.; Li, L.; Xu, Z.; Sun, H.; Amin, S.; Guo, F.; Shi, W.; Li, Y. Engineering of 2D/3D architectures type II heterojunction with high-crystalline g-C₃N₄ nanosheets on yolk-shell ZnFe₂O₄ for enhanced photocatalytic tetracycline degradation. *Mater. Res. Bull.* **2022**, *150*, 111789. [[CrossRef](#)]
125. Li, Y.; Qin, T.; Chen, W.; Huang, M.; Xu, J.; Lv, J. Construction of a Switchable g-C₃N₄/BiVO₄ Heterojunction from the Z-Scheme to the Type II by Incorporation of Pyromellitic Diimide. *Cryst. Growth Des.* **2022**, *22*, 1645–1653. [[CrossRef](#)]
126. Sundararaj, S.B.; Amir, H.; Viswanathan, C.; Thangavelu, S. Photoelectrochemical Water Splitting: A Visible-Light-Driven CoTiO₃@g-C₃N₄-Based Photoanode Interface Follows the Type II Heterojunction Scheme. *Langmuir* **2024**, *40*, 16582–16594. [[CrossRef](#)]
127. Maridevaru, M.C.; Nagaveni, M.; Kumari, M.M.; Shankar, M.V.; Khraisheh, M.; Selvaraj, R. Unravelling the efficiency of CoAl-LDH/g-C₃N₄ nanosheets: Type-II heterojunction for photocatalytic hydrogen production and dye degradation under solar light irradiation. *Int. J. Hydrogen Energy* **2024**, *89*, 1112–1125. [[CrossRef](#)]

128. Wang, C.; Kong, X.; Yu, Z.; Tao, X.; Huang, L.; Shang, S. Construction of g-C₃N₄/Fe-MOFs Type-II heterojunction promotes photo-Fenton degradation of doxycycline. *Sep. Purif. Technol.* **2023**, *326*, 124790. [[CrossRef](#)]
129. Omori, F.; Tateishi, I.; Katsumata, H.; Furukawa, M.; Kaneco, S. Fabrication of pyridine incorporated and O-doped g-C₃N₄/COF: A type-II heterojunction for enhanced hydrogen production under visible light irradiation. *J. Solid State Chem.* **2025**, *341*, 125057. [[CrossRef](#)]
130. Gao, C.; Sun, Y.; Yu, S.; Liu, L.; Liu, C.; Li, Y.; Wang, H.; Chang, X. Type-II heterojunction Se-g-C₃N₄/ZnO coupled MnCo₂O₄ photocatalyst for enhanced levofloxacin hydrochloride degradation activated by peroxymonosulfate. *Chem. Eng. J.* **2024**, *500*, 156944. [[CrossRef](#)]
131. Song, B.; Wang, Q.; Wang, L.; Lin, J.; Wei, X.; Murugadoss, V.; Wu, S.; Guo, Z.; Ding, T.; Wei, S. Carbon nitride nanoplatelet photocatalysts heterostructured with B-doped carbon nanodots for enhanced photodegradation of organic pollutants. *J. Colloid Interface Sci.* **2020**, *559*, 124–133. [[CrossRef](#)] [[PubMed](#)]
132. Balu, S.; Chen, Y.-L.; Chen, S.-W.; Yang, T.C.K. Rational synthesis of BixFe_{1-x}VO₄ heterostructures impregnated sulfur-doped g-C₃N₄: A visible-light-driven type-II heterojunction photo(electro)catalyst for efficient photodegradation of roxarsone and photoelectrochemical OER reactions. *Appl. Catal. B-Environ.* **2022**, *304*, 120852. [[CrossRef](#)]
133. Bard, A.J. Photoelectrochemistry and heterogeneous photo-catalysis at semiconductors. *J. Photochem.* **1979**, *10*, 59–75. [[CrossRef](#)]
134. Low, J.; Yu, J.; Jaroniec, M.; Wageh, S.; Al-Ghamdi, A.A. Heterojunction Photocatalysts. *Adv. Mater.* **2017**, *29*, 1601694. [[CrossRef](#)]
135. Tada, H.; Mitsui, T.; Kiyonaga, T.; Akita, T.; Tanaka, K. All-solid-state Z-scheme in CdS-Au-TiO₂ three-component nanojunction system. *Nat. Mater.* **2006**, *5*, 782–786. [[CrossRef](#)] [[PubMed](#)]
136. Yu, J.; Wang, S.; Low, J.; Xiao, W. Enhanced photocatalytic performance of direct Z-scheme g-C₃N₄-TiO₂ photocatalysts for the decomposition of formaldehyde in air. *Phys. Chem. Chem. Phys.* **2013**, *15*, 16883–16890. [[CrossRef](#)] [[PubMed](#)]
137. Wang, Z.; Meng, S.; Li, J.; Guo, D.; Fu, S.; Zhang, D.; Yang, X.; Sui, G. Oxygen Vacancy Engineering and Constructing Built-In Electric Field in Fe-g-C₃N₄/Bi₂MoO₆ Z-Scheme Heterojunction for Boosting Photo-Fenton Catalytic Degradation Performance of Tetracycline. *Small* **2024**, *20*, 2406125. [[CrossRef](#)]
138. Zheng, D.; Pang, C.; Wang, X. The function-led design of Z-scheme photocatalytic systems based on hollow carbon nitride semiconductors. *Chem. Commun.* **2015**, *51*, 17467–17470. [[CrossRef](#)]
139. Liu, X.; Cai, L. A novel double Z-scheme BiOBr-GO-polyaniline photocatalyst: Study on the excellent photocatalytic performance and photocatalytic mechanism. *Appl. Surf. Sci.* **2019**, *483*, 875–887. [[CrossRef](#)]
140. Iwase, A.; Ng, Y.H.; Ishiguro, Y.; Kudo, A.; Amal, R. Reduced Graphene Oxide as a Solid-State Electron Mediator in Z-Scheme Photocatalytic Water Splitting under Visible Light. *J. Am. Chem. Soc.* **2011**, *133*, 11054–11057. [[CrossRef](#)]
141. Li, X.; Sun, H.; Xie, Y.; Liang, Y.; Gong, X.; Qin, P.; Jiang, L.; Guo, J.; Liu, C.; Wu, Z. Principles, synthesis and applications of dual Z-scheme photocatalysts. *Coord. Chem. Rev.* **2022**, *467*, 214596. [[CrossRef](#)]
142. Wang, G.; Cheng, H. Recyclable MXene-bridged Z-scheme NiFe₂O₄/MXene/Bi₂WO₆ heterojunction with enhanced charge separation for efficient sonocatalytic removal of ciprofloxacin. *Sci. Total Environ.* **2023**, *901*, 165833. [[CrossRef](#)] [[PubMed](#)]
143. Ma, R.; Su, Y.; Li, C.; Lv, X.; Li, W.; Yang, J.; Zhang, W.; Wang, H. Novel MOF-derived dual Z-scheme g-C₃N₄/Bi₂O₂CO₃/β-Bi₂O₃ heterojunctions with enhanced photodegradation of tetracycline hydrochloride. *Sep. Purif. Technol.* **2025**, *354*, 128580. [[CrossRef](#)]
144. Fu, J.; Xu, Q.; Low, J.; Jiang, C.; Yu, J. Ultrathin 2D/2D WO₃/g-C₃N₄ step-scheme H₂-production photocatalyst. *Appl. Catal. B-Environ.* **2019**, *243*, 556–565. [[CrossRef](#)]
145. Zhu, B.; Cheng, B.; Fan, J.; Ho, W.; Yu, J. g-C₃N₄-Based 2D/2D Composite Heterojunction Photocatalyst. *Small Struct.* **2021**, *2*, 2100086. [[CrossRef](#)]
146. Zhang, L.; Zhang, J.; Yu, H.; Yu, J. Emerging S-Scheme Photocatalyst. *Adv. Mater.* **2022**, *34*, 2107668. [[CrossRef](#)]
147. Hao, P.; Chen, Z.; Yan, Y.; Shi, W.; Guo, F. Recent advances, application and prospect in g-C₃N₄-based S-scheme heterojunction photocatalysts. *Sep. Purif. Technol.* **2024**, *330*, 125302. [[CrossRef](#)]
148. Duan, X.; Yang, J.; Zhu, J.; Li, H.; Fang, Y.; Liu, R.; Yang, C.; Liu, W.; Ding, C.; Liu, Q.; et al. Activated CdS/sulfur doped g-C₃N₄ photocatalyst for dye and antibiotic degradation: Experimental and DFT verification of S-scheme heterojunction. *Environ. Res.* **2025**, *266*, 120487. [[CrossRef](#)]
149. Kumar, A.; Khosla, A.; Sharma, S.K.; Dhiman, P.; Sharma, G.; Gnanasekaran, L.; Naushad, M.; Stadler, F.J. A review on S-scheme and dual S-scheme heterojunctions for photocatalytic hydrogen evolution, water detoxification and CO₂ reduction. *Fuel* **2023**, *333*, 126267. [[CrossRef](#)]
150. Zhao, S.; Jiang, J.; Zhang, C.; Chen, F.; Song, Y.; Tang, Y. Construction of a novel double S-scheme heterojunction CeO₂/g-C₃N₄/Bi₂O₄ for significantly boosted degradation of tetracycline: Insight into the dual charge transfer mode. *Chem. Eng. J.* **2024**, *479*, 147333. [[CrossRef](#)]
151. Che, L.; Pan, J.; Cai, K.; Cong, Y.; Lv, S.-W. The construction of p-n heterojunction for enhancing photocatalytic performance in environmental application: A review. *Sep. Purif. Technol.* **2023**, *315*, 123708. [[CrossRef](#)]

152. Chen, W.; Huang, J.; He, Z.; Ji, X.; Zhang, Y.-F.; Sun, H.; Wang, K.; Su, Z. Accelerated photocatalytic degradation of tetracycline hydrochloride over CuAl₂O₄/g-C₃N₄ p-n heterojunctions under visible light irradiation. *Sep. Purif. Technol.* **2021**, *277*, 119461. [[CrossRef](#)]
153. Wang, L.; Dong, Y.; Zhang, J.; Tao, F.; Xu, J. Construction of NiO/g-C₃N₄ p-n heterojunctions for enhanced photocatalytic CO₂ reduction. *J. Solid State Chem.* **2022**, *308*, 122878. [[CrossRef](#)]
154. Feng, Q.; Liu, Z.; Su, R.; Chen, Y.; Wang, Y.; Ma, D.; Li, Q. Revealing the reaction mechanism of the novel p-n heterojunction Mn₃O₄-C₃N₄ in efficient activation of chlorite to degrade organic pollutants under piezoelectric catalysis. *Appl. Catal. B-Environ.* **2025**, *362*, 124714. [[CrossRef](#)]
155. Yang, S.; Wu, T.; Li, K.; Huang, P.; Li, W.; Zhuo, Y.; Liu, K.; Yang, Z.; Han, D. Photocatalytic Enhancement and Recyclability in Visible-Light-Responsive 2D/2D g-C₃N₄/BiOI p-n Heterojunctions via a Z-Scheme Charge Transfer Mechanism. *Molecules* **2024**, *29*, 5418. [[CrossRef](#)]
156. Dharani, S.; Gnanasekaran, L.; Arunachalam, S.; Zielinska-Jure, A.; Almoallim, H.S.; Soto-Moscoso, M. Photodegrading rhodamine B dye with cobalt ferrite-graphitic carbon nitride (CoFe₂O₄/g-C₃N₄) composite. *Environ. Res.* **2024**, *258*, 119484. [[CrossRef](#)]
157. Zhan, X.; Zeng, Y.; Zhang, Z.; Xia, Y.; Xu, J.; Hong, B.; Wang, X. G-C₃N₄ with gradient vacancies to enhance spatial charge carriers transfer and separation for photodegrading antibiotics under visible light. *Chem. Eng. J.* **2023**, *474*, 145948. [[CrossRef](#)]
158. Wang, X.; Zhu, Z.; Jiang, J.; Li, R.; Xiong, J. Preparation of heterojunction C₃N₄/WO₃ photocatalyst for degradation of microplastics in water. *Chemosphere* **2023**, *337*, 139206. [[CrossRef](#)]
159. Qiu, J.; Wang, D.; Chang, Y.; Feng, Q.; Liu, Z.; Pang, M.; Meng, D.; Feng, Y.; Fan, C. Anchoring single-atom Cu on tubular g-C₃N₄ with defect engineering for enhanced Fenton-like reactions to efficiently degrade carbamazepine: Performance and mechanism. *Chem. Eng. J.* **2024**, *479*, 147841. [[CrossRef](#)]
160. Liu, Z.; Liu, Y.; Sun, X.; Ji, H.; Liu, W.; Cai, Z. Construction of Z-scheme Ag/AgVO₃/carbon-rich g-C₃N₄ heterojunction for enhanced photocatalytic degradation of sulfamethiazole: DFT calculation and mechanism study. *Chem. Eng. J.* **2022**, *433*, 133604. [[CrossRef](#)]
161. Qin, L.; Meng, J.; Yang, G.; Pan, Y.; Gao, X.; Yang, Y.; Guo, Y. Interlayer single-atomic Fe-N₄ sites on carbon-rich graphitic carbon nitride for notably enhanced photo-Fenton-like catalytic oxidation processes towards recalcitrant organic micropollutants. *Appl. Catal. B-Environ. Energy* **2024**, *345*, 123695. [[CrossRef](#)]
162. Manh Dung, N.; Thanh Binh, N.; Linh Hai, T.; Thuy Giang, N.; Fatimah, I.; Kuncoro, E.P.; Doong, R.-A. Z-scheme S, B co-doped g-C₃N₄ nanotube@MnO₂ heterojunction with visible-light-responsive for enhanced photodegradation of diclofenac by peroxymonosulfate activation. *Chem. Eng. J.* **2023**, *452*, 139249. [[CrossRef](#)]
163. Cheng, Z.; Ling, L.; Wu, Z.; Fang, J.; Westerhoff, P.; Shang, C. Novel Visible Light-Driven Photocatalytic Chlorine Activation Process for Carbamazepine Degradation in Drinking Water. *Environ. Sci. Technol.* **2020**, *54*, 11584–11593. [[CrossRef](#)] [[PubMed](#)]
164. Xiao, J.; Xie, Y.; Rabeah, J.; Brueckner, A.; Cao, H. Visible-Light Photocatalytic Ozonation Using Graphitic C₃N₄ Catalysts: A Hydroxyl Radical Manufacturer for Wastewater Treatment. *Acc. Chem. Res.* **2020**, *53*, 1024–1033. [[CrossRef](#)]
165. Sun, Y.; Fang, Z.; Huang, X.; Bai, C.; Zhu, K.; Chen, X.; Zhang, B.; Zhang, Y.; Yang, Q.; Zheng, J.; et al. Efficient photo-switchable activation of periodate by nitrogen-vacancy-rich carbon nitride for organic contaminant removal: Theoretical predictions and experimental validations. *Appl. Catal. B-Environ.* **2023**, *337*, 122994. [[CrossRef](#)]
166. You, Q.; Zhang, C.; Cao, M.; Chen, P.; Wang, B.; Wang, Y.; Huang, J.; Deng, S.; Yu, G. Coordinating the exciton-mediated and carrier-mediated photocatalytic mechanisms of carbon nitride using acetylacetone for enhancing emerging contaminants removal. *Appl. Catal. B-Environ. Energy* **2023**, *338*, 123025. [[CrossRef](#)]
167. Zhang, B.; Xia, S.; Wang, Z.; Li, W.; Li, B.; Zhang, H.; Xin, Y.; Wu, K.; Ma, J.; He, X. Enhanced permanganate activation by g-C₃N₄ under visible light irradiation: Unraveled mechanism involving Mn(V) and photo-induced electron. *Appl. Catal. B-Environ. Energy* **2024**, *349*, 123861. [[CrossRef](#)]
168. Yu, Z.; Wu, J.; Zhang, J.; Chen, X.; Wang, Z.; Zhang, Y.; Li, D.; Chen, J.; Liu, H.; Chen, P.; et al. Carbon nitride nanotubes anchored with Cu(I) triggers peracetic acid activation with visible light for removal of antibiotic contaminants: Probing mechanisms of non-radical pathways and identifying active sites. *J. Hazard. Mater.* **2023**, *460*, 132401. [[CrossRef](#)]
169. Zhang, B.; Kong, L.; Yan, X.; Zhang, H.; Wang, Z.; Xia, S.; Han, Z.; Xin, Y.; Ding, A.; Ma, J.; et al. Recent progress in graphitic carbon nitride-based catalysts for water treatment: Contaminant elimination, disinfection and membrane applications. *Sep. Purif. Technol.* **2025**, *354*, 129420. [[CrossRef](#)]

Disclaimer/Publisher's Note: The statements, opinions and data contained in all publications are solely those of the individual author(s) and contributor(s) and not of MDPI and/or the editor(s). MDPI and/or the editor(s) disclaim responsibility for any injury to people or property resulting from any ideas, methods, instructions or products referred to in the content.